

1 **Observations of the temporal variability in aerosol properties and their relationships to**
2 **meteorology in the summer monsoonal South China Sea/East Sea: The scale-dependent**
3 **role of monsoonal flows, the Madden-Julian Oscillation, tropical cyclones, squall lines and**
4 **cold pools.**
5

6 Jeffrey S. Reid¹, Nofel D. Lagrosas², Haflidi H. Jonsson³, Elizabeth A. Reid¹, Walter R.
7 Sessions⁴, James B. Simpas², Sherdon N. Uy², Thomas J. Boyd⁵; Samuel A. Atwood⁶; Donald
8 R. Blake⁷, James R. Campbell¹, Steven S. Cliff⁸, Brent N. Holben⁹, Robert E. Holz¹⁰, Edward J.
9 Hyer¹, Peng Lynch¹¹, Simone Meinardi⁷, Derek J. Posselt¹², Kim A. Richardson¹, Santo V.
10 Salinas¹³, Alexander Smirnov¹⁴, Qing Wang³, Liya Yu¹⁵, Jianglong Zhang¹⁶.

11
12 [1] {Marine Meteorology Division, Naval Research Laboratory, Monterey CA}

13 [2] {

14 [Manila Observatory, Ateneo de Manila University, Quezon City, Philippines](#)

15 ~~[Manila Observatory, Manila Philippines](#)~~}

16 [3] {Department of Meteorology, Naval Postgraduate School, Monterey CA}

17 [4] {CSC, Naval Research Laboratory, Monterey CA}

18 [5] {Biogeochemistry Section, Naval Research Laboratory, Washington DC}

19 [6] {Dept. of Atmospheric Science, Colorado State University, Ft. Collins, CO}

20 [7] {University of California, Irvine, CA}

21 [8] {University of California, Davis, CA}

22 [9] {NASA Goddard Space Flight Center}

23 [10] {Space Sciences Engineering Center, University of Wisconsin, Madison, WI}

24 [11] {CSC Inc. at Naval Research Laboratory, Monterey CA}

25 [12] {Dept. of Atmospheric, Oceanic, and Space Sciences, University of Michigan, Ann Arbor,

26 MI}

27 [13] {Centre for Remote Imaging Sensing and Processing, National University
28 of Singapore, Singapore}

29 [14] {Sigma Space Corporation, Lanham, MD}

30 [15] {Dept. of environmental Engineering, National University of Singapore, Singapore}

31 {National University of Singapore, Singapore}

32 [16] {Dept. of Meteorology, University of North Dakota, Grand Forks, ND}

33

34 Correspondence to: J. S. Reid (jeffrey.reid@nrlmry.navy.mil; 1 831-656-4725)

35

36

37 ABSTRACT: In a joint NRL/Manila Observatory mission, as part of the 7 SouthEast Asian
38 Studies program (7SEAS), a two-week, late September 2011 research cruise in the northern
39 Palawan Archipelago was undertaken to observe the nature of southwest monsoonal aerosol
40 particles in the South China Sea/East Sea (SCS/ES) and Sulu Sea region. Previous analyses
41 suggested this region as a receptor for biomass burning from Borneo and Sumatra for boundary
42 layer air entering the monsoonal trough. Anthropogenic pollution and biofuel emissions are also
43 ubiquitous, as is heavy shipping traffic. Here, we provide an overview of the regional
44 environment during the cruise, a time series of key aerosol and meteorological parameters, and
45 their interrelationships. Overall, this cruise provides a narrative of the processes that control
46 regional aerosol loadings and their possible feedbacks with clouds and precipitation. While 2011
47 was a moderate El Nino/Southern Oscillation (ENSO) La Nina year, higher burning activity and
48 lower precipitation was more typical of neutral conditions. The large-scale aerosol environment
49 was modulated by the Madden Julian Oscillation (MJO) and its associated tropical cyclone (TC)
50 activity in a manner consistent with the conceptual analysis performed by *Reid et al.*, (2012).
51 Advancement of the MJO from phase 3 to 6 with accompanying cyclogenesis during the cruise
52 period strengthened flow patterns in the SCS/ES that modulated aerosol lifecycle. TC inflow
53 arms of significant convection sometimes span from Sumatra to Luzon, resulting in very low
54 | particle concentrations (minimum condensation nuclei $CN < 150 \text{ cm}^{-3}$, non-sea salt $PM_{2.5} \leq 1 \mu\text{g m}^{-3}$).
55 | m^{-3}). However, elevated carbon monoxide levels were occasionally observed suggesting passage
56 | of polluted air masses whose aerosol particles had been rained out. Conversely, two drier periods
57 | occurred with higher aerosol particle concentrations originating from Borneo and Southern
58 | Sumatra ($CN > 3000 \text{ cm}^{-3}$ and non-sea salt $PM_{2.5} 10\text{-}25 \mu\text{g m}^{-3}$). These cases corresponded with
59 | two different mechanisms of convection suppression: lower free-tropospheric dry-air intrusion
60 | from the Indian Ocean, and large-scale TC-induced subsidence. Veering vertical wind shear also
61 | resulted in aerosol transport into this region being mainly in the marine boundary layer (MBL),
62 | although lower free troposphere transport was possible on the western sides of Sumatra and
63 | Borneo. At the hourly time scale, particle concentrations were observed to be modulated by
64 | integer factors through convection and associated cold pools. Geostationary satellite observations
65 | suggest that convection often takes the form of squall lines, which are bowed up to 500 km
66 | across the monsoonal flow and 50 km wide. These squall lines, initiated by cold pools from large
67 | | thunderstorms and likely sustained by a veering vertical wind shear and aforementioned mid
68 | | troposphere dry layers, propagated over 1500 km across the entirety of the SCS/ES-effectively
69 | cutting large swaths of MBL aerosol particles out of the region. Our conclusion is that while
70 | large-scale flow patterns are very important in modulating convection and hence allowing long
71 | range transport of smoke and pollution, more short-lived phenomena can modulate cloud
72 | condensation nuclei (CCN) concentrations in the region, resulting in pockets of clean and
73 | polluted MBL air. This will no doubt complicate large scale comparisons of aerosol-cloud
74 | interaction.
75

76

77 1.0 INTRODUCTION

78 Given its hypothesized sensitivity to global climate change (e.g., IPCC 2007; Yusuf and
79 Francisco 2009), Southeast Asia (SEA) has experienced a substantial increase in scientific
80 interest; from the region’s highly complex meteorology, to its atmospheric chemistry, air quality,
81 and climate. The region, including the Maritime Continent, South China Sea/East Sea (SCS/ES),
82 and Sulu Sea, is thought to be highly susceptible to aerosol cloud interactions (Rosenfeld, 1999;
83 Hamid et al., 2001; Yuan et al., 2011). Indeed, around the second half of the boreal summer
84 monsoonal period from August to mid-October, the seasonal dry climate allows biomass burning
85 throughout the Maritime Continent (MC), particularly in warm El Nino-Southern Oscillation
86 phases (e.g, Nichol 1998; van der Werf et al., 2004; Field and Shen 2008; Langner and Siegert
87 2009; Field et al., 2009; van der Kaars et al., 2010; Reid et al., 2012; 2013). Climatologically,
88 there exists both anecdotal evidence and some station data suggesting an increase in the number
89 of no-rain days in the Philippines (Cruz et al., 2013), yet perhaps an increase in intense events
90 (Cinco et al., 2014). Perhaps such a behavior is as a result of the effect of increasing aerosol
91 emissions on ~~small cumulus~~ clouds. At the same time there is a long-standing hypothesis that
92 there are increases in mid-level cloudiness, also perhaps due to increased levels of aerosol particles
93 (Parungo et al., 1994).

94

95 Under most circumstances, smoke and pollution from the MC is thought to be transported by
96 southwesterly monsoonal winds into the SCS/ES where it is scavenged by convection ~~or~~ with
97 eventual annihilation in the monsoonal trough (Reid et al., 2012; Xian et al., 2013). However, the
98 transition process between “polluted land” and “clean monsoonal trough” is poorly understood.
99 Large scale modeling studies suggesting smooth transport are at odds with visible imagery (Reid
100 et al., 2013) and lidar observations (e.g., Campbell et al., 2013), which suggest smoke is often
101 sequestered on or very near the major land masses. Owing to near ubiquitous high cloud cover in
102 the SCS/ES, there are relatively few satellite observations of smoke transport in the region,
103 except during anomalously clear or severe events. The limited remote sensing data that are
104 available is largely qualitative, with both cloud and aerosol retrievals showing great regional
105 diversity across product lines in this near-ubiquitous cloud environment (Reid et al., 2013).
106 While higher-frequency meteorological phenomena, such as the Madden Julian Oscillation and
107 equatorial waves (Reid et al., 2012), as well as orographic and sea breeze effects, are thought to

108 exert significant influence on transport (*Mahmud, 2009a,b; Reid et al., 2012; Wang et al., 2013;*
109 *Xian et al., 2013*), there are virtually no in situ observations of the SCS/ES aerosol environment
110 in this critical summer monsoonal season. Cloud processes in regions such as the MC are
111 expected to be sensitive to the presence of aerosol particles (e.g., *Sorooshion et al., 2009; Yuan et*
112 *al., 2011; Lee et al., 2012*). But, we have little information on how well models perform.

113
114 As part of the 7 Southeast Asian Studies (7SEAS) program (*Reid et al., 2013*), a two-week
115 research cruise was conducted from September 17- 30, 2011 in the northern half of the Palawan
116 Archipelago of the Philippines; a region thought to be a long range receptor for MC biomass
117 burning and industrial emissions (*Reid et al., 2012; Xian et al., 2013*). At the same time,
118 additional sun photometer, lidar and ground measurements were made in Singapore to contrast
119 with the Philippine receptor. Other sun photometers were located across Southeast Asia.
120 Conducted on the M/Y *Vasco*, a locally owned 35 m vessel, our goals were to make first-ever (to
121 our knowledge) measurements of near-surface aerosol properties in the region, test the transport
122 hypotheses put forth in *Reid et al. (2012)*, and develop new hypotheses on aerosol-weather
123 interaction that regulate aerosol prevalence to be studied in future deployments. *Most*
124 *importantly, we aim to develop a narrative on how model simulations and remote sensing*
125 *retrievals correspond with real world observations in this highly complex aerosol and*
126 *meteorological environment.* Often, the intricacies of aerosol-meteorological relationships are
127 blurred in bulk analyses to the detriment of understanding regional physics and chemistry. Only
128 through studies, such as presented here, can we hope to derive the true sensitivity of the region to
129 aerosol emissions.

130
131 In this paper, we give a brief overview of the cruise and its measurements, as well as other
132 regional measurements made to aid in interpreting the regional aerosol environment. This will
133 form a descriptive basis for subsequent 7SEAS papers on aerosol and cloud features for the 2011
134 burning season, as well as a contrast to a similar 2012 cruise to be reported at a later date. The
135 analysis portion of this paper is focused on the temporal variability of aerosol particle number
136 and mass concentrations and how these relate to regional meteorological phenomenon, such as
137 large scale monsoonal flow, the MJO, TC development and propagation, and large scale squall
138 lines/cold pools. We end with a discussion of the strong covariance between aerosol prevalence

139 and regional thermodynamic behavior, noting how it must be considered in studies of aerosol,
140 cloud, and precipitation interaction.

141

142 2.0 CRUISE DESCRIPTION AND INSTRUMENTATION

143 This research cruise was conducted on the 35 meter, 186 ton M/Y *Vasco*, owned and operated by
144 Cosmix Underwater Research Ltd. Manila, Philippines. Photos of the vessel along with its cruise
145 track are provided in Figure 1. The *Vasco* departed on Sept. 17, 2011 from Navotas, Manila Bay,
146 and returned midday Sept. 30. The target area for the bulk of the monitoring was in the vicinity
147 of El Nido and outside of Malampaya Sound, Palawan Island (Lat=111.1N; Long=119.3E). The
148 general mode of operation was to travel to selected areas, then choose locations for sampling
149 which had a clear breeze to the open ocean, though protected from the sometimes large swell
150 with no local wave breaking. Great care was taken to not position the ship downwind of any
151 sources. Indeed, small settlements are ubiquitous on small islands. But these were all avoided.

152 The ship would move every one to two days within each area to support other physical
153 oceanographic measurements. The route south from Manila included a one-day stop at Apo Reef
154 on Sept. 18, and the coast of Culion on September 19. From Sept. 20 through the morning of
155 September 28th the *Vasco* operated in the northern Palawan area. On the morning of Sept. 29th,
156 the *Vasco* departed El Nido for return to Manila on the early afternoon of Sept. 30th.

157

158 Instrumentation was generally deployed in two configuration groups. Self-contained
159 instrumentation, including meteorology and aerosol chemistry, was located on a 3 m flux tower
160 on the bow of the ship; a total top-to-bottom height of 6 m above the ocean surface. This ensured
161 no self-contamination from the ship except for very rare periods of a following wind. Aerosol
162 particle counters and nephelometers were located in a forward locker fed by a 4 cm diameter/4 m
163 long inlet from the top of the ship. Wind directional data ensured only periods with air moving
164 over the bow were used (to remove periods of contamination and self-sampling from the
165 dataset). Periods of self-sampling were also abundantly clear from CN counts. Such periods were
166 obvious-with rapid particle count fluctuations in the 1000 to 10,000+.

167

168 2.1 Meteorology

169 The meteorological instrumentation set was associated with the 3 m flux tower. While fluxes are

170 a subject of a separate paper, a brief summary is appropriate here. A Campbell sonic anemometer
171 and Licor IR H₂O/CO₂ system were sampled at 50 hz to provide fluxes of momentum, sensible
172 and latent heat. Mean meteorology was also provided by an RM Young propeller anemometer
173 and a Campbell pressure and ventilated temperature and humidity probe. Sea surface temperature
174 was provided by a waterline floating thermocouple. Downwelling shortwave radiation was
175 measured with a Kipp and Zonan CMP 22 radiometer. Ship location and attitude were given by a
176 Garmin GPS and accelerometer package. This attitude and velocity data was used to correct
177 meteorology and solar radiation data.

178

179 In addition to the flux tower, ceiling and visibility were provided by a Vaisala C31 ceilometer,
180 which has been shown to provide information on aerosol particle profiles when properly
181 corrected (e.g., *Clarke et al.*, 2003; *Markowicz et al.*, 2008; *Tsaknakis et al.*, 2011). Twenty-five
182 InterMet 1-AB radiosondes were also released during the cruise, generally one to two per day;
183 twenty of these passed our quality control. Forward-looking automatic cameras logged images
184 every minute.

185

186 2.2 Aerosol and Gas Chemistry

187 A series of aerosol samplers were mounted on the bow of the ship. One of the primary
188 instruments utilized in this paper was a free-standing eight-stage Davis Rotating-drum Uniform
189 size-cut Monitor (DRUM) sampler. The instrument used in this study was a version of the
190 DRUM sampler originally described by *Cahill et al.* (1985), modified to utilize slit orifices and
191 configured to run at 16 L min⁻¹ as described in *Reid et al.* (2008). A similar instrument was
192 deployed for comparison to Dongsha Island in the SCS/ES in 2011 in the winter/ spring
193 Northeasterly Monsoon (*Atwood et al.*, 2013a). An unheated PM₁₀ sample inlet was used
194 upstream of the impactor, followed by collection stages with nominal 50% aerodynamic
195 diameter-cut sizes of 5 μm, 2.5 μm, 1.15 μm, 0.75 μm, 0.56 μm, 0.34 μm, 0.26 μm, and 0.07
196 μm. Aerosol particles were collected on Mylar strips coated with Apiezon grease and wrapped
197 around each rotating drum. The drums were rotated at a consistent rate such that nominal
198 timestamps could be assigned to specific locations along the strip during compositional analyses,
199 yielding 90 minute time resolution. DRUM samples were subjected to X-Ray Fluorescence
200 (XRF) analysis at the Advanced Light Source (ALS) of Lawrence Berkeley National Laboratory

201 to provide measurements of selected elements having atomic weights between Mg and Mo, along
202 with Pb. Unlike previous DRUM analyses described in the literature, the XRF Analysis samples
203 for this study utilized a more advanced detector system, making XRF derivations of key sea salt
204 elements, such as Na and Cl much more quantitative. For simplicity here, time series of
205 elemental concentration data for the eight raw size fractions were combined into two lumped size
206 fractions: Coarse (stages 1-3 or 10-1.15 μm in aerodynamic size), and fine (stages 4-8, or 1.15-
207 0.07 μm), respectively. A more detailed analysis will be provided by a forthcoming paper by
208 *Lagrosas et al. (2014 – manuscript in preparation)*.

209
210 $\text{PM}_{2.5}$ filters were also collected in daily 5 lpm Minivol Tactical Air Samplers (TAS) and
211 analyzed by gravimetric, XRF and ion chromatography at the Desert Research Institute. A
212 second set of filters provided organic and black carbon, by the method of Chow et al. (1993).
213 Finally, PM_{10} and 2.5 samples were collected by the Manila Observatory using both TAS and a
214 three-stage Dylec impactor for gravimetric and ion chromatography analysis. These, too, are
215 discussed in *Lagrosas et al. (~~2014~~2015 – manuscript in preparation)*.

216
217 For trace-gas analysis, forty-six whole air gas samples were collected in electro-polished
218 stainless steel cans for analysis by gas chromatography by the University of California Irvine.
219 See Colman et al. (2001) for details, a full list of 60+ compounds, and relative uncertainties.
220 However, only a few species are presented here (e.g., CO, and few halo and hydrocarbons).
221 Flame ionization detectors (FIDs) were used to measure C_2 - C_{10} hydrocarbons, electron capture
222 detectors (ECDs) were used for C_1 - C_2 halocarbons and C_1 - C_5 alkyl nitrates, and quadrupole mass
223 spectrometer detectors (MSD) were used for unambiguous compound identification and selected
224 ion monitoring. Cans were supplied for the cruise under vacuum, and upon valve release at the
225 ship's bow under headwind, each collected its volume over the course of ~20 seconds.
226 Measurement precision varied by species, but was better than 5% for the vast majority of
227 species. The most uncertain was dibromochloromethane at 8%. Cans were opened sporadically
228 throughout the cruise, with at least two samples a day being collected generally in the morning
229 and afternoon. Sampling was generally not performed during rain showers. Additional cans were
230 sampled during excellent or interesting sampling conditions, with the highest frequency during
231 the last few days when the ship was a receptor for smoke. Of the forty-six can samples, five did

232 not pass quality assurance as they had anomalously high hydrocarbon and solvent levels. Given
233 the collection procedure, based over the side on the windward bow of the ship, we are not
234 entirely sure how the contamination may have happened, but suspect it may reflect some local
235 contaminant from the scattered islands in the region. For the purposes of this paper on large scale
236 flow, they are excluded here.

237

238

239 2.3 Ship Aerosol Microphysics and Optics

240 Onboard the *Vasco* were a particle counter, sizers, and a nephelometer. Total particle
241 concentrations were measured by a TSI Water Condensation Nuclei Counter (CPC). Fine and
242 coarse-mode particle size was provided by a DMT bench top Passive Cavity Aerosol Sizing
243 Spectrometer (PCASP), and a TSI Aerodynamic Particle Sizer which were calibrated before and
244 after the cruise. These low-flow rate instruments were behind a dry-rite drying column, which
245 dropped relative humidity to ~50%. However, while the CPC and APS operated without incident,
246 the PCASP suffered a relay failure after the first night at sea (night of Sept 17). This was repaired
247 by Sept 24th for the second half of the cruise.

248

249 For light scattering, we used a TSI three-wavelength nephelometer ($\lambda=445, 550, 700$ nm) at
250 ambient RH, and corrected for truncation/non-lambertian light source errors using Anderson et
251 al. (1996). A three-wavelength Particle Soot Absorption Photometer (PSAP) sampled from the
252 nephelometer stream, and was corrected via *Bond et al.* (1999). A Radiance Research single
253 wavelength nephelometer ($\lambda=532$) was also placed downstream of the drying column. Finally, a
254 Microtops hand-held sun photometer was brought on board as part of the Maritime Aerosol
255 Network (MAN; Smirnov et al., 2011) for measuring Aerosol Optical Thickness (AOT).
256 However, cloudy skies prohibited measurements prior to the last two days of the cruise (Sept 29
257 and 30). Comprehensive studies of aerosol optical properties and size are a subject of a
258 subsequent paper. However, here we use the CPC and PCASP to show time series of basic fine-
259 mode particle number and size properties.

260

261 2.4 Regional AERONET Measurements.

262 In addition to the *Vasco* cruise, a number of other instruments were placed in the region to help
263 monitor the aerosol environment. Most notable, in reference to this paper, was a set of four
264 AERONET sun photometers (*Holben et al.*, 1998), located on the map in Figure 2b. Two sites
265 including the Singapore 7SEAS super site (e.g., *Atwood et al.*, 2013b), Kuching, Sarawak Borneo
266 (*Salinas et al.*, 2013) and Marbel University, Mindanao, Philippines were set up for 7SEAS.
267 Songkhla, Thailand was pre-existing operational. For the purposes of this paper, we focus one
268 parameter, 500 nm daily averaged fine-mode AOT. This was generated from the Level 2.0
269 Spectral Deconvolution Algorithm (SDA) Version 4.1, used to separate fine and coarse-mode
270 contributions to AOT (*O'Neill et al.*, 2003). By using the SDA, we can effectively remove thin
271 cirrus contamination (*Chew et al.*, 2011) and focus on fine-mode particles from industrial and
272 biomass burning sources.

273

274 2.5 Ancillary Satellite and Model Data

275 Baseline meteorology data are provided by the Navy Global Atmospheric Prediction System
276 (NOGAPS; *Hogan and Rosmond*, 1991). We compared NOGAPS fields to NCAR reanalysis
277 fields (*Kalnay et al.*, 1996) for the individual events discussed in this paper and, as we found no
278 substantive differences, NOGAPS data are subsequently used for initializing the offline Navy
279 Aerosol Analysis and Prediction System (NAAPS). NAAPS, the Navy's operational aerosol
280 model, is a global operational 1° x 1° aerosol transport model supporting various operations and
281 research, including the monitoring of biomass burning plumes (*Reid et al.*, 2009). NAAPS has
282 been extensively exercised for the Maritime Continent region (e.g., *Hyer and Chew*, 2010; *Reid*
283 *et al.*, 2012; *Xian et al.*, 2013). The emissions, transport, and sinks of sulfate combined pollution
284 product (particulate organic matter plus sulfates), open biomass burning smoke, and dust are
285 simulated, and quality-assured AOT retrievals from MODIS observations are assimilated into the
286 model (*Zhang et al.*, 2008). Model output includes predicted speciated mass concentrations and
287 AOT. The NAAPS data were used to provide a regional assessment, as well as along the ship
288 track.

289

290 To establish mid and upper-troposphere air-mass source regions, and the large scale flow pattern
291 for selected periods of the cruise, back trajectories were generated using the NOAA Hybrid
292 Single Particle Lagrangian Integrated Trajectory (HYSPLIT) Version 4.9 Model (*Draxler &*

293 Hess, 1997, 1998; Draxler, 2004). The GDAS1, $1^\circ \times 1^\circ$ global meteorological dataset, generated
294 for HYSPLIT from the Global Data Assimilation System model, was used to run 72 hr
295 backwards trajectories.

296
297 Numerous satellite products (visible, IR, cloud heights, scatterometer, etc.) are also used in an
298 imaging capacity to aid in the analyses. These can all be found on the NEXSAT system (Miller *et*
299 *al.*, 2006; <http://www.nrlmry.navy.mil/nexsat-bin/nexsat.cgi>) and are cited as used in this paper.

300 We also use other retrieved products for context, such as the Climate Prediction Center (CPC)
301 MORPHing technique (CMORPH, Joyce *et al.*, 2004) for precipitation and derived data
302 assimilation-grade satellite AOT products from MODIS (Zhang *et al.*, 2008) and MISR (Kahn *et*
303 *al.*, 2009). MODIS fire counts are also used here, following the regional interpretation of Hyer *et*
304 *al.* (2013). While it would have been highly valuable, CALIPSO data were not collected during
305 the cruise period due to solar anomalies. However, we do present a single collect from Oct. 1 in
306 conditions we believe to be representative of the last few days of the cruise.

307
308 3.0 RESULTS I: REGIONAL METEOROLOGICAL AND AEROSOL CHARACTERISTICS

309 The *Vasco* cruise occurred in the second half of the month of September, 2011. This period is
310 typically towards the end of the boreal summer southwest monsoon (henceforth SWM) system,
311 approximately two to three weeks before the transition period to boreal winter/spring northeast
312 monsoon (NEM). A general overview of the summer monsoonal system can be found in Chang
313 *et al.* (2005), Moron *et al.* (2009) and the book by Chang *et al.* (2011). An overview of how
314 monsoonal weather features relate to smoke emissions and transport from progressively larger to
315 finer scales can be found in Reid *et al.*, (2012); Xian *et al.*, (2013), Mahmud (2009a,b) and Wang
316 *et al.*, (2013), respectively. A brief description of key meteorological and aerosol elements for the
317 summer 2011 burning season, as they relate to the study measurement period, is provided here.

318 *3.1 Overall Nature of the Meteorological and Aerosol Environment.*

319 As discussed in the references above, the SWM in the greater Southeast Asian region is generally
320 between mid-April and mid-October. Associated lower-atmospheric flows in the MC are easterly
321 when south of 3°S , and westerly when north of this latitude. In the SCS/ES, surface winds turn
322 southwesterly, eventually terminating in a monsoonal trough east of the Philippines. In the upper
323 free troposphere over the SCS/ES, winds flow in the opposite direction to the marine boundary

324 layer and lower free troposphere: generally north-easterly, originating from the monsoonal
325 trough. The ~500 hPa level generally is the delineation between southwest winds below and
326 northeast winds above. Winds at these mid-levels are generally light.

327 For the purposes of this paper, the general meteorology during the cruise is depicted in Figure
328 2(a), where NOGAPS surface and 850 hPa winds (black & magenta, respectively) are provided.
329 These two levels bound the vast majority of aerosol particles in the region during the SWM
330 (*Tosca et al.*, 2011; *Campbell et al.* 2013; *Chew et al.*, 2013; *Wang et al.*, 2013). Average study
331 period precipitation from CMORPH is also provided as the color background. The red star in the
332 northern Palawan area indicates the *Vasco's* position during the bulk of the sampling. Figure 2(b)
333 provides a map of all MODIS (Terra+Aqua) fire counts during the study period. Here, green stars
334 indicate relevant AERONET sun photometer data utilized in this study. Finally, Figure 2(c)
335 provides the average MODIS + MISR AOTs for the mission, although readers should be aware
336 that AOTs in the northern half of the domain were derived from only the last few days of the
337 study when skies were clear enough to perform a retrieval (this is discussed in more detail later).

338 The wind fields in the SCS/ES during the study period were largely typical for the SWM season,
339 with its prevailing southwesterly winds, averaging ~8-20 m s⁻¹ over most of the region. The
340 transition from easterlies and southeasterlies south of the equator to southwesterlies in the
341 SCS/ES can be seen in the general wrapping of the winds around Borneo and Sumatra. Wind
342 strength anomalies were generally low over the region, although in the middle of the SCS/ES
343 positive anomalies were on the order of 7 m s⁻¹. Clear cyclonic activity in the northern SCS/ES
344 region is also apparent. As we discuss later, these positive wind anomalies are result of TC
345 activity and inflow arm wind enhancement during the cruise. Also notable is the slight veering
346 wind shear at lowest levels. While the surface winds are clearly southwesterly, they do become
347 more westerly through the lower free troposphere to 700 hPa. As discussed later, this has
348 significant implications for regional aerosol transport and convection.

349 Precipitation is a maximum along the monsoonal trough, which extends from the northern
350 SCS/ES to the southeast. However, during the mission, precipitation was not continuous in this
351 region, but was rather a composite of enhanced local precipitation, lows, squall lines and tropical
352 cyclone development. Secondary precipitation maxima were visible and include 1) convection
353 over land; 2) precipitation west of Sumatra in the so called West Sumatran Low, and 3)

354 convection east of Myanmar driven by convergence of oceanic air masses reaching land. A
355 depiction of the diversity of regional cloud features during the mission can be seen in Fig. 3. An
356 area of ~~total-near~~ absence of precipitation south of southern Borneo and southern Sumatra except
357 for isolated mountain top convection, encompassing such islands as Java and Timor, is a
358 common feature of the SWM.

359 The 2011 season corresponded to a moderate La Nina year (Multivariate ENSO Index= -0.95).
360 This typically implies higher precipitation and less fire activity than normal (*Field and Shen*
361 2008; *Field et al.*, 2009; *Reid et al.*, 2012). However, in this particular year, precipitation and fire
362 activity were more characteristic of a neutral year. Thus, while fire activity and smoke AOTs
363 were not akin to the boreal summer El Nino events of 1997, 2004, 2006 and 2009, 2011 ranks in
364 the middle third in our estimate of fire activity since 2000 (based on *Reid et al.*, 2012 statistics).
365 As is typical for the late SWM, fire activity was concentrated in southern Sumatra and southern
366 Borneo/Kalimantan. Fires in this region are often associated with peatland burning, although a
367 great deal of plantation and small holder slash burning is common (See *Reid et al.*, 2013 for a
368 discussion of regional burning practices). As actual peat burning is much more common in
369 drought years (e.g., *Field and Shen*, 2008; *Miettinen et al.*, 2010; 2011), we suspect much of the
370 observed burning was associated with agricultural maintenance or deforestation.

371 Intermediate fire activity corresponded with moderate AOT in the region, as can be seen in Fig.
372 2(c) that provides average composites of MISR and MODIS (Terra+Aqua) AOT. Near the
373 biomass burning sources, AOTs can be high, averaging over 1 for $\lambda=550$ nm. This is likely low-
374 biased, as AOT retrievals often flag thick aerosol plumes as cloud in the region (*Reid et al.*,
375 2013). Comparison of the Figure 2 panels elucidates regional transport patterns: smoke generated
376 in Sumatra and Borneo is carried by the southwesterly winds through the SCS/ES and eventually
377 scavenged out. Some Sumatran smoke also crosses the island's western mountain range and
378 enters the Indian Ocean. While model representation of regional smoke transport often suggests a
379 smooth transition, imagery, and both passive satellite and lidar observations, often depict a strong
380 gradient between island and ocean (e.g., *Campbell et al.*, 2013; *Reid et al.*, 2012, 2013).
381 Prevailing hypotheses for this divergence surround scale-dependent issues in the model, and the
382 reproducibility of orographic and sea breeze meteorology (e.g., *Reid et al.*, 2012; *Wang et al.*,
383 2013; *Xian et al.*, 2013). But overall, the transport and transformation mechanisms from polluted

384 island to clean marine background air are not well understood nor easily simulated. This paper,
385 as well as subsequent efforts based on this cruise, hope to address these problems.

386 3.2 Evolution of the meteorological environment during the Vasco cruise

387 The timing of the *Vasco* cruise was serendipitous, as it coincided with the transition of the MJO
388 from wetter to a drier phase in the MC. The MJO is a large-scale, coupled pattern of meso-
389 synoptic scale circulation and deep convection that forms in the Indian Ocean and propagates
390 eastward at $\sim 5 \text{ m s}^{-1}$ through and around the MC and into the Pacific Ocean (*Madden and Julian*,
391 1971; *Zhang*, 2005, 2014). Phase and amplitude of the MJO are quantified for this study using
392 the method of *Wheeler and Hendson* (2004). Once this convective region passes into the
393 central/eastern Pacific and decays, a new event may start in the Indian Ocean, repeating the
394 cycle. From an aerosol point of view, while ENSO is an excellent large-scale indicator of
395 seasonal burning, the wet and dry phases of the MJO strongly influence the intraseasonal timing
396 of significant smoke events in the MC (*Reid et al.*, 2012). While the MJO was hypothesized to
397 influence overall AOT (*Tian et al.*, 2008), no satellite-based AOT verification of this has yet been
398 established due to the difficulty in performing aerosol remote sensing in the region (*Reid et al.*,
399 2013). However, fire observations are strongly enhanced in dry phases (*Reid et al.*, 2012) and
400 mechanistically a relationship between dry MJO phase, fire emissions, and high AOT seems
401 highly likely certain.

402
403 An important correlation of MJO-related convection as it transits and departs the MC is an
404 associated increase in the formation of regional TCs (*Maloney and Hartman*, 2001). *Reid et al.*,
405 (2012) noted that when TCs transit the SCS/ES there is an increase in both fire activity in the
406 southern MC and ventilation of smoke into the SCS/ES region. This relationship is thought to be
407 associated with an acceleration of southwesterly winds in the SCS/ES as air approaches the TC.
408 As TCs enter the area, strong convection develops along the inflow arm, scavenging smoke
409 transported offshore. Later, as the TC passes, large-scale subsidence follows, resulting in
410 negative precipitation anomalies over much of the SCS/ES and MC. An example of such a case
411 is presented in global and mesoscale simulations in *Reid et al.* (2012) and *Wang et al.* (2013),
412 respectively. Over the period of Sept 17-30, the MJO convective active phase migrated out of the
413 MC (that is migrated from Phase 3 to Phase 6) at a relative strength that increased above the one

414 standard deviation intensity level halfway through the period. The migration of the MJO
415 coincided with a train of TC activity beginning Sept 23.

416 Select examples of daily mean winds with precipitation and representative daytime MTSAT
417 visible images are found in Figures 3(a)&(b), respectively. On Sept 17, the day of departure, the
418 general meteorology of the SCS/ES and MC was fairly typical for a convectively-active phase of
419 the MJO. Regional lower-tropospheric winds exhibited small anomalies against the NCEP
420 climatology. Comparison of the CMORPH-derived precipitation (Figure 3(a)) with MTSAT
421 visible images (Figure 3(b)) suggested the whole region was showery, with light scattered
422 precipitation from many small to medium-sized cells and a few deep and intense storms. Some
423 organization can be seen, however, in an 800 km wide area in the SCS/ES between southern
424 Vietnam and Borneo. Over the next forty-eight hours (Sep 19), precipitation over the region
425 increased, and the patch of convection in the SCS further organized and intensified. By Sept 22,
426 convection intensified further over the whole SCS/ES, and cyclonic rotation became clearly
427 evident around a tropical depression in the northern SCS. This coupled system resulted in lines
428 of convection and heavier precipitation from the southwest to the northeastern side of the
429 SCS/ES. The tropical depression was later named Tropical Storm 21 W- Haitang. Haitang
430 continued developing until Sep 25th, reaching maximum winds of 18 m s⁻¹. The inflow arm of
431 Haitang moved westward, leaving the southern SCS/ES drier.

432 As Haitang was beginning to develop, a separate system, 20 W Nesat, rapidly intensified in the
433 western Pacific Ocean and migrated westward. As Haitang then migrated into northern Vietnam,
434 Nesat developed, making landfall on Luzon on Sep 26 with maximum one-minute sustained
435 wind speeds of ~58 m s⁻¹ –ultimately listed as a Category 4 TC. After passing Luzon and causing
436 an estimated \$1B damage, Nesat lost strength to Category 1 before making landfall again at
437 Hunan Island on September 29. Finally, the third tropical cyclone, the westward-tracking
438 Typhoon #22W Nalgae made landfall in northern Luzon as a more compact but stronger
439 Category 4 storm (67 m s⁻¹ sustained) on October 1. Detailed discussion of these storms can be
440 found in the Joint Typhoon Warning Center Annual Tropical Cyclone Report
441 (<http://www.usno.navy.mil/NOOC/nmfc-ph/RSS/jtwc/atcr/2011atcr.pdf>)

442 These three tropical storms changed the nature of the regional meteorology for the second half of
443 | the cruise, and as we discuss, modulated regional aerosol loadings. Satellite imagery clearly

444 showed the region oscillating between significant convection, developing in inflow arms (e.g.,
445 Sept. 22 & 27) across the SCS/ES, followed by areas of considerable clearing (e.g., Sept 24-25 &
446 29-30). Inflow arms corresponded with increases in southwesterly winds, perhaps further
447 ventilating MC air into the SCS/ES region.

448

449 *3.3 Evolution of the overall aerosol environment during the Vasco cruise period*

450 To provide context to regional fire and aerosol behavior during the *Vasco* cruise, time series of
451 fire activity and AOTs are given in Figure 4. Figure 4(a) shows the MODIS fire hotspot time
452 series for key regions in the MC for the 2012 burning season. As explained in *Reid et al.* (2012)
453 to account for satellite orbit, some smoothing of the data are required; in this case a 5 day boxcar
454 is used. Four fire events are visible over the course of the SWM. First, an early-season event in
455 late July/early August is visible in Central Sumatra and Indonesian Kalimantan (predominately
456 western Kalimantan); this is associated with early agricultural burning. A second and much more
457 significant peak in late August is found in Southern Sumatra and Indonesian Kalimantan
458 provinces predominately in the south. This is fairly anomalous behavior, especially for a La Nina
459 year, as this region typically burns very late in the season (*Reid et al.*, 2012).

460

461 In September, two more events, one early and one late in the month, are visible. The first,
462 peaking around September 7th is region wide, but is dominated by Sumatra. The last major event,
463 which corresponded with the *Vasco* cruise, peaked September 26th, with major contributions
464 from southern Sumatra and Kalimantan and more minor contributions from islands to the south
465 of Borneo. As noted in *Reid et al.* (2012), these peaks in observed fire activity often correspond
466 to dry MJO phases (e.g., Aug. 23, Sept. 26) or overall weak MJO activity (e.g., Sept. 5). The
467 period of July 20- August 8 corresponded with a late-phase MJO event. A new MJO event
468 formed August 18. We suspect drying ahead of the convective portion of the event perhaps
469 allowed southern Kalimantan to burn more readily on August 23rd. The wettest phase of the MJO
470 (phase 3) was in the MC from Aug 28-Sept 18. A break in precipitation in the southern MC
471 allowed the Sept 8th fire event, which was dominated by southern Sumatra, and the border of
472 more significant precipitation to the north. It is emphasized, however, that while we believe plots
473 such as Figure 4(a) are indicative of qualitative fire patterns, they are nevertheless influenced by
474 clear sky bias, which also corresponds with MJO activity.

475

476 While the MC generally has high background aerosol concentrations from pervasive industrial,
477 shipping and biofuel sources (*Reid et al.*, 2013), peaks in AOTs from AERONET sites largely
478 match fire activity. Fine-mode AOT from four sites are shown in Figure 4: (b) Singapore; (c)
479 Songkhla (further up the Malay Peninsula in peninsular Thailand), (d) Kuching in Sarawak
480 Malaysia, Borneo, and e) Notre Dame of Marbel University on Mindanao. Fine mode AOTs
481 from sites near sources typically ranged from 0.1-0.3 during background conditions, and 0.4-1.0
482 during biomass burning events. For the most part, the August 23rd event was the largest region
483 wide, with significant spikes in both Singapore (impacted from Sumatra) and Kuching (impacted
484 largely by southern Kalimantan). The September 7th event is also visible in Singapore, but there
485 is little indication of smoke over Kuching. The *Vasco* cruise period captured the last AERONET
486 AOT peaks for the season in Singapore, Kuching and in particular Mindanao. This establishes
487 that the ship was well positioned as a long range receptor for transport from the MC into the SW
488 monsoonal trough.

489 Because of the generally small fraction of clear sky, frequent high thin clouds, and sometimes
490 extreme AOTs in the region, it is difficult to apply satellite AOT retrievals in a straightforward
491 manner. In particular, sampling bias can be pervasive (*Zhang and Reid*, 2009). However, the
492 AOT analyses in Figure 4 that are associated with the meteorological modes presented in Section
493 3.2 are illustrative of regional aerosol loadings: (f) MJO Active phase: Sept 17-22; (g) MJO
494 transition and TC active phase: Sept 23-27; and (h) post TC environment and clearing: Sept 28-
495 30. These AOT maps, coupled with the large-scale flow patterns shown in Figure 2&3, are
496 suggestive of a large-scale southwesterly transport event from the MC to the SCS/ES region in
497 the latter half of the cruise. Early in the cruise, while burning was at a minimum, moderate AOTs
498 still existed in the vicinity of Sumatra and Borneo. Air was relatively clean north of the equator.
499 During the development of the TC active phase, the accelerated burning resulted in a two-to-
500 three factor increase in observed AOTs in the source regions. Smoke ~~is clearly visible~~ being
501 transported into the SCS/ES, Celebes Sea, and Sulu Sea is clearly visible. Due to clearing in the
502 post TC phase, retrievals were then possible over much of the region. Heavy smoke is observed
503 as far as 10° N, with moderate AOTs extending past Luzon. Cleaner air masses with AOT<0.125
504 are clearly visible on the western side of the Philippines Thus, from the time series in both Figs.
505 2 and 4, we would expect aerosol concentrations to increase as air masses entered the convective

506 regions of the SCS/ES. As no satellite retrievals were ever made on the track of the *Vasco*, a
507 question remains as to the aerosol concentrations within the active regions. This is addressed in
508 the next section where we discuss environmental time series from the *Vasco*.

509 From an aerosol modeling perspective, Figure 5 presents a time series of AOT, surface
510 anthropogenic fine-mode concentrations, and biomass burning provided by the NAAPS
511 reanalysis for key transitional days. Through use of AOT data assimilation and satellite
512 precipitation to constrain wet deposition, this is a reliable global model scale perspective of
513 aerosol transport in this data sparse region. Shown are four of the days in Figure 3: Sep 18, 22,
514 24, and 30. By and large, modeled aerosol fields match our expectations from the meteorology.
515 While AOTs are high near source areas in the first half of the cruise, convection over the SCS/ES
516 quickly scavenged aerosol particles near shore. This was particularly true for periods with well-
517 established TC inflow arms. In the second half of the cruise, ~~associated with clearer periods,~~ two
518 strong injection and transport events carried aerosol particles as far north as Luzon. These events
519 were separated by TC Nesat. The relative strengths of anthropogenic pollution versus biomass
520 burning suggest significant burning enhancement ~~and regional~~ in the last days of the cruise. Of
521 particular note is that in the middle portion of the cruise, model and flow data suggest the
522 northern Palawan region was most dominated by transport up the SCS/ES from the Java Sea and
523 Southeastern Borneo, with the Sulu Sea being dominated by transport from eastern Borneo
524 through the Celebes Sea. This Sulu Sea flow pattern then dominated for the last few days of the
525 cruise, although as discussed in the next section, we suspect some additional industrial sources in
526 the final day.

527 Finally, aerosol vertical distribution is a crucial element of the system. Unfortunately, CALIPSO
528 was placed in standby mode from Sep 22-30 due to solar flare activity. For the early cruise (Sept.
529 17-22) thick regional cirrus cover and orbital track conspired to prevent meaningful aerosol data
530 collections. However, the NAAPS reanalysis does provide a simulation of aerosol vertical
531 distribution, and we checked for consistency once CALIPSO data was made available for Oct. 1st
532 when cirrus optical thickness was low enough to profile the aerosol layers underneath. These
533 data are presented in Figure 6. Meridional cross sections for total fine-mode aerosol particle
534 concentration are provided for Sept. 24 and 30, for 110° and 120°E longitude across the SCS/ES
535 and Sulu Sea regions. These meridians are marked on the AOT plots of Figure 5. At Borneo and

536 immediate outflow regions, NAAPS generally keeps the bulk of the aerosol mass concentration
537 below 3 km, in line with previous remote sensing (*Tosca et al.*, 2011; *Campbell et al.*, 2013) and
538 higher resolution modeling efforts and comparison (*Wang et al.*, 2013). We can interpret this as
539 smoke mixing through a deep planetary boundary layer, including the PBL cloud entrainment
540 zone. This deep layer progresses well offshore east of Borneo in the Celebes Sea. However, as
541 we go further into the SCS/ES and Sulu Sea, fine-mode aerosol particles concentrations are
542 increasingly predominant in the lowest kilometer.

543 CALIOP data in Figure 6, collected on Oct. 1, 2011 (the day after the *Vasco* returned to port but
544 still probably representative of the second large event), shows the same features, with perhaps an
545 aerosol layer aloft at 1-2 km in North Western Borneo, but a sharp aerosol layer below 1 km
546 across the SCS/ES region. In this case, the scale heights are even lower than NAAPS, perhaps
547 due to numerical diffusion in the vertical in the model. This regional transition from deeper to
548 shallower aerosol scale height, as one moves out in the SCS/ES, is seen very clearly in
549 climatological [lidar](#) data (e.g., *Campbell et al.*, 2013). In the context of this cruise, we can
550 explain it as a result of the veering wind shear in the lowest portion of the atmosphere. Aerosol
551 particles in the MBL are transported with a more southwesterly wind. At 850 hPa and above,
552 winds are more westerly. Thus, aerosol particles ~~at higher~~ these levels are transported eastward
553 rather than north. Similarly, convective lofting into the lower troposphere will then place the
554 aerosol particles in a westerly wind, and thus any northward component of transport must be
555 associated with the MBL. This finding makes understanding the sea breeze induced ejection of
556 smoke on the western side of Borneo all the more important in the simulation of smoke transport
557 to the Philippines and the monsoonal trough. For eastward transport off of eastern Borneo, the
558 boundary layer and lower free troposphere winds have similar directions. Hence, we find deeper
559 aerosol layers in the Celebes Sea. Based on the climatological aspects of wind shear (e.g., *Reid et*
560 *al.*, 2012), we expect this generally explains the climatological aerosol vertical distribution in the
561 region ~~presented by~~ *Campbell et al.*, (2013). This finding also suggests that the surface sampling
562 by the *Vasco* was largely indicative of smoke and pollution transport, and is representative.

563 4.0 RESULTS II: VASCO METEOROLOGY AND AEROSOL TIME SERIES

564 As Section 3 has established the overall nature of the lower troposphere, we can begin to
565 interpret the measurement time series from the *Vasco*. In particular, we wish to understand how

566 the large-scale conceptual models and observations presented above relate to real world marine
567 boundary layer meteorology and aerosol phenomena. Key meteorological and aerosol
568 measurements, which best depict the overall environment, are presented in Figure 7. Included are
569 the meteorological parameters: (a) pressure; (b) temperature; (c) wind speed; (d) wind direction;
570 and (e) precipitation rate. Key aerosol parameters include (f) the 30-min average water CPC total
571 aerosol concentration; (g) the estimated PM_{2.5} mass concentrations from filters (corrected to
572 remove sea salt by subtracting sea salt based on 3.26* Na concentration) and organic and black
573 carbon from quartz filters. Also shown are grab-can samples of CO; (h) PM₁ ammonium sulfate
574 (NH₄)₂SO₄ in red (based on DRUM sampler S assuming all non-sea salt S was in (NH₄)₂SO₄)
575 with coarse-mode sea salt in blue (1-10 μm, based on the Na*3.26 method), and finally (i)
576 NAAPS-derived total fine-mode particle concentration, differentiated between biomass burning
577 and a combined interactive anthropogenic +biogenic product.

578 Marked on Figure 7 are points of interest during the cruise to be discussed herein. They begin
579 with departure from Manila Harbor, followed by our exit from Manila Bay. Our first point of
580 stationary sampling was at Apo Reef, followed the next day at the West Coron site. Long time-
581 period stationary sampling was then conducted at Guntao Island just outside of El Nido, then just
582 outside Malampaya Sound, and then back at Guntao Island again. During the last Guntao Island
583 measurement period, the *Vasco* experienced the largest cold pool event, a topic of discussion of
584 Section 4.2. Late on Sept 26, the *Vasco* took shelter from Typhoon Nesat in Liminangcong
585 harbor, which showed considerable local contamination. Once there was suitable reduction in
586 significant wave heights, the *Vasco* moved north to just outside El Nido harbor to enable more
587 regional sampling, ~~although some local sources may still have influenced the data~~. On the
588 morning of September 29, the *Vasco* had to return to Manila harbor via the Mindoro Strait ahead
589 of TC Nalgae. In preparation for Nalgae, our equipment was shut down and boxed up one third
590 of the way into Manila Bay midday on Sept 30.

591 Based on a preliminary analysis of NAAPS data (e.g., Figure 5), boundary layer air sources were
592 all coastal Borneo or Southern Sumatra/Java Sea for most of the cruise. The two important
593 exceptions were in the first day and last two days of the cruise, when model and trajectories
594 suggest some influence from northern Borneo the Celebes Sea. As discussed above, winds
595 veered with height, with the lower free-tropospheric air tracing an origin to the Malay Peninsula

596 and Indian Ocean, where pollution and biomass burning emissions are significantly reduced.
597 Thus, we expect highest particle concentrations to be in the MBL.

598 4.1 Daily scale meteorological and aerosol concentration features

599 To understand the nature of the coupled meteorological-aerosol environment we have to
600 reconcile large scale meteorological and remote sensing analyses with the data at a single
601 receptor point (i.e., *Vasco*). Clearly from Figure 7, both the meteorology and atmospheric
602 composition observed on the cruise are a convolution of low to high frequency signals. To begin
603 the analysis, we consider features with scale of a day or longer.

604
605 As we would expect for a tropical region, overall we see a large measure of consistency in many
606 meteorological features. At daily scales, pressure is relatively constant for the cruise with the
607 exception of a moderate dip ~Sept 26-29 associated with TC Nesat and an embedded diel-solar-
608 tidal signal. Baseline temperatures are also constant at ~28°C, with a 2°C dip also associated with
609 heavy rains from the TC. Surface winds were generally 5-10 ms⁻¹ and typically from the
610 Southwest with occasional departure to the north. Precipitation was showery throughout, with
611 precipitation visible in some form most days, but with the most significant events in the outer
612 rain bands associated with TC Nesat. Embedded in these daily scale features are clear high-
613 frequency phenomena; for example, inverse ramp drops in temperature, with associated spikes in
614 wind speed, and often precipitation. As discussed in Section 4.2, such high-frequency
615 phenomena are largely associated with convective cells and their associated cold pools.

616
617 Within the cruise, we see several large-scale aerosol features. Certainly, just before the *Vasco* left
618 Manila Harbor and Bay, we observed a high spike in particulate matter, indicative of local
619 pollution. However as the *Vasco* departed, we entered a cleaner greater-bay regime, upwind of
620 Manila Bay sources. Outside of Manila Bay, a spike in particulate matter was also observed,
621 likely due to local Luzon influence such as from Batangas. “Regional” SCS/ES monitoring was
622 initiated with the *Vasco*’s first anchorage at Apo Reef in Mindoro Strait on September 18. A more
623 typical background period was observed through midday Sept. 22nd, followed by a significant
624 aerosol event ~Sept 24rd – 26th ended by the arrival of TC Nesat. A second even larger event then
625 followed from late Sept 28 through the return on Sept 30th.

626

627 From the Apo Reef to the northern Palawan anchorages on September 23rd, the *Vasco* was in a
628 very clean aerosol regime. CN counts were generally on the order of $\sim 300\text{-}500\text{ cm}^{-3}$, and non-sea
629 salt $\text{PM}_{2.5}$ was $\sim 2\text{ }\mu\text{g m}^{-3}$. PM_{10} sea salt was on the order of $5\text{ }\mu\text{g m}^{-3}$. Both fine and coarse
630 particle mass are in line with expectations in a background marine atmosphere (Quinn et al.,
631 1996; Henintzenberg et al., 2000; Reid et al., 2006). On Sept 22nd, particle concentrations
632 reached a mission minimum, with sustained CN concentrations below 150 cm^{-3} , and non-sea salt
633 $\text{PM}_{2.5} < 1\text{ }\mu\text{g m}^{-3}$; at or below our minimum detectable limits. Coarse-mode sea salt remained
634 relatively constant, increasing slightly to $6\text{ }\mu\text{g m}^{-3}$. During this time period, however, we found
635 variable CO grab sample data ranging from 80-118ppbv, uncorrelated with particle properties.
636 This first period can be explained through the development of TC Haitang near the SCS/ES, and
637 the formation of a broad southwest to northeast inflow arm on Sept 22 clearly visible in Figure 3.
638 As the inflow arm developed, winds accelerated and precipitation from both shallow and deep
639 convective cells increased. Thus, while Borneo/Java Sea air was clearly being transported to the
640 *Vasco* receptor, precipitation scavenged most fine particles, leaving insoluble trace gases but few
641 particles. Pulses of slightly-enhanced CO nevertheless reached the ship. NAAPS correctly
642 captures this period as relatively clean, although total mass concentrations are high by $\sim 2\text{-}3\text{ }\mu\text{g}$
643 m^{-3} .

644
645 The first observed regional aerosol event having a clear Indonesian or Malay source was initiated
646 on Sept. 23, when Haitang moved westward, leaving clearer skies and lighter winds. The *Vasco*
647 remained at the same anchorage outside of El Nido for this entire event. This period saw a slow
648 development in particle concentrations and CO and was largely precipitation free. Non-sea salt
649 $\text{PM}_{2.5}$ was on average $8\text{-}9\text{ }\mu\text{g m}^{-3}$, with black carbon and organic carbon mass fractions on the
650 order of 5 and 20%, respectively. Corresponding CN counts were on the order of $1000\text{-}2000\text{ cm}^{-3}$.
651 This period also corresponded with reduced surface winds across the SCS/ES, and an
652 associated slight reduction in coarse-mode sea salt. A significant dip in particle concentrations
653 and temperature was observed late Sept 24th UTC ($\sim 3\text{ AM}$ local time), which, as we discuss in
654 Section 4.2, was associated with a strong trans-SCS/ES convection-cold pool event. Finally, fine
655 particle mass concentrations reached a maximum and then fell precipitously with the arrival of
656 storm conditions associated with TC Nesat. NAAPS identified this event well as a mixture of
657 anthropogenic and biomass burning sources, although total fine-mode mass concentration is

658 overrepresented by ~30%. We suspect this is a result of a low bias in the NOGAPS RH field,
659 which in the context of AOT data assimilation well upstream of the *Vasco*, results in an
660 overestimation of dry mass relative to ambient scattering.

661
662 During the storm period, the *Vasco* was in safe harbor at Liminangcong; the high and variable
663 CN are due to local harbor emissions. After TC Nesat passed, the *Vasco* returned to El Nido for a
664 day of measurements and eventual departure back to Manila. This cruise return period was
665 associated with very light winds and the highest observed particle concentrations, perhaps with a
666 Borneo source. Again, such fair weather is expected on the back side of a strong tropical cyclone
667 such as Nesat, and was further reinforced with the impending arrival of another Category 4
668 storm, TC Nalgae (Figure 3, Sep 30). Fortunately, the typical southwesterly winds slackened to
669 such an extent that the ships own velocity kept air moving over the bow, thus avoiding self-
670 sampling that would have ruined the return period dataset. A time-series analysis of model and
671 trajectory shows that, leading up to this event, transport associated with the last vestiges of the
672 TC Nesat's influence in accelerating regional winds brought the air mass up to the sampling
673 region. Due to wind shear, it is possible it included contributions from both western and eastern
674 Borneo. While we cannot dismiss the possibility of local contamination in the gas can samples
675 while we were in safe harbor in Liminangko, we do see a steady increase in CO reaching a
676 plateau during the final event.

677
678 As the *Vasco* left El Nido, black and organic carbon mass fractions were on the order of 5% and
679 40% suggestive of biomass burning dominance. This period also afforded the only cirrus-free
680 conditions for Microtops sun photometry measurements. 500 nm AOTs were on the order of
681 0.30, very similar to the MODIS retrievals shown in Figure 4(h). NAAPS also captured this
682 event well, and yielded a correct 0.3 AOT. However, like the previous event, total particle
683 concentrations are biased high. Again, we suspect this is due to a low bias in the NOGAPS RH
684 fields. Even so, NAAPS suggests a significant enhancement in biomass burning particle
685 concentrations relative to anthropogenic pollution.

686
687 Based on back trajectories, NAAPS simulations, and particle concentrations, one would initially
688 be inclined to believe the *Vasco* sampled one air mass on its return to Manila. However,

689 examination of wind data shows westerly to northerly winds at the very end of the mission. This
690 plus chemistry (Section 4.4 and Lagrosas et al., [20142015](#), *manuscript in preparation*) show that
691 in the last six hours of the cruise there are slight perturbations to the sources, perhaps a change in
692 the mixture of biomass burning and industrial pollution or the addition of a regional shipping
693 signal. Indeed, across the horizon on Sept 30 we saw many high polluting vessels with plumes
694 visible from 10-30 km away.

695
696 A final consideration for large scale observations is how aerosol loading covaries with
697 atmospheric soundings, perhaps influencing interpretation of aerosol, cloud and precipitation
698 interaction studies. Figure 8 presents three example cases where we found isolated convection,
699 Sept 18th, 25th, and 29th. Sept 18 was our first stop at Apo Reef, where we observed relatively
700 clean aerosol conditions and isolated convection. Over the twenty-four hour period we observed
701 many warm rain events with significant precipitation, as shown in Figure 8(a) & 7(e). For
702 intermediate pollution on September 25th, we encountered significant amounts of boundary layer
703 clouds, but little precipitation (Figure 8 (b); Figure 7(e)). On the other end of the spectrum, Sept
704 29th was indicative of polluted conditions where there were few boundary layer clouds, but
705 occasional significant convection (Figure 8 (c); Figure 7(e)). Simple correlation studies and
706 current scientific thinking would suggest these cases epitomized aerosol-cloud-precipitation
707 interactions. That is, in clean conditions, we have significant amounts of warm rain. If aerosol
708 particle concentrations are perturbed from background conditions, warm rain ceases, and perhaps
709 there is enhancement in severe cells. However, as demonstrated in Figure 8(d)-(f), atmospheric
710 soundings were very different for these cases. Being the tropics, one expects relatively
711 conditionally-stable potential temperature profiles, which indeed we found to be largely the case
712 (Figure 8(d)). But, we can see that for the polluted Sept 25th case, a clear stronger inversion is
713 present at 700 hPa. This inversion corresponds with a lower free-tropospheric dry layer between
714 900-700 hPa with both halved water vapor mixing ratio (Figure 8(e)) and relative humidity
715 (Figure 8(f)). This certainly impaired the development of warm rain formation, even without
716 possible aerosol effects. For the most significant biomass burning event (Sept 29th), the PBL was
717 drier than was typical, yet the lower troposphere was relatively moist. But in this case, large TC
718 induced subsidence produced a dry layer in the mid to upper troposphere, strongly capping
719 convection.

720 To better understand the nature of dry stable layers, Figure 9(a)&(b) present back trajectories
721 initiated at the key “dry altitudes” of 1.6 km (850 hPa) and 6.8 km (500 hPa), respectively, for
722 our cases of Sept. 18, 25 and 29. Tick marks are located every twenty-four hours, and time-
723 height dependencies are provided. For the lower free troposphere, we see clear differences
724 between Sept. 18th and the 25th & 29th, with the 18th originating from convection off of Borneo.
725 For both the 25th and 29th, the lower-to-middle free tropospheric air originated in the Indian
726 Ocean. The NOGAPS time-height cross section over the Phuket, Thailand radiosonde site clearly
727 shows a dry air intrusion into the region between 2 and 5 km (900 and 600 hPa). This may be
728 related to subsidence behind the propagating MJO. Nevertheless, it does demonstrate how
729 dynamics in the Indian Ocean and the formation of dry layers can be coupled to SCS/ES and
730 Sulu Sea convection and their aerosol environment. In regard to upper-level subsidence,
731 trajectories are highly divergent, but show significant lifting and subsidence associated with the
732 passage of TCs.

733

734 *4.2 High Frequency Squall Line and Cold Pools Phenomenon*

735 Embedded in the Figure 7 time series are clear, sharp perturbations in both meteorological and
736 aerosol features. Most significant of these are drops in temperature on the order of 2-5 °C within
737 minutes, and even here we must consider the response time of the aspirated temperature probe.
738 With the drop in temperature, there was a sharp spike in wind speed, relative humidity and at
739 times precipitation, and a drop in particle concentration and water vapor mixing ratio. These
740 characteristics are indicative cold pool events related to convective downdrafts (*Wakimoto* 1985;
741 *Atkins and Wakimoto* 1991; *Miller et al.*, 2008; *Zuidema et al.*, 2012). Over twenty such events
742 are observable in the time series, with significant variability in amplitude. Recovery from the
743 drop in temperature and particle concentration to the pre-event baseline ranged from one to ten
744 hours. Some of these events originated from what were clearly local isolated cells. However,
745 investigation of the largest such events suggest that they originate in long-lived squall lines,
746 propagating in the monsoonal flow and initiated from the cold pools of massive thunderstorms
747 over land or along the coast. This phenomenon appears to be extremely important for
748 determining aerosol fate in this region, and deserves detailed study in its own right. For this
749 study, we will limit our discussion to the most significant event observed during the cruise.

750

751 The pathology of SCS/ES organized squall line/cold pool phenomena best described by the
752 cruise data was for a Sept 24th event in the middle of the first significant aerosol transport
753 episode. Key aspects of the Sept 24th event are presented in Figure 10 as one-minute averages.
754 Included are (a) a time series of temperature and wind speed; (b) relative humidity and pressure;
755 (c) PCASP and CPC total particle count; and PCASP (d) number and (e) volume size
756 distributions. The cold pool hit at 16:28 UTC (corresponding to 00:28 LST on Sept 25th). Wind
757 cup speed accelerated from the background 7-8 m s⁻¹ to 14 ms⁻¹ within the first two seconds, with
758 flux estimates of gusts at the two-to-five second level to 25 m s⁻¹ within the next fifty seconds.
759 Winds then momentarily subsided to 5 ms⁻¹ for the next ten minutes, followed by another
760 increase and decrease over the next hour, and a slow recovery. Corresponding with the wind
761 onset was a ~5°C drop in temperature, and increase in relative humidity over the first minutes,
762 although there was only a minor 0.2 hPa perturbation in pressure. Sea surface temperature
763 dropped 0.2°C and recovered only after sunrise. Approximately 1 cm of precipitation occurred
764 over a one-hour period, initiated fifteen minutes after gust front arrival, breaking the wind lull.
765 Maximum precipitation rate was on the order of 4 cm hr⁻¹. Surface particle concentrations
766 dropped precipitously with cold pool arrival: PCASP counts dropping from ~700 cm⁻³ to 300 cm⁻³
767 ¹ within two minutes, followed by a further reduction to 150 cm⁻¹ at precipitation onset. CPC
768 dropped from ~1450 to 400 cm⁻¹. An interesting feature was a clear enhancement in coarse-mode
769 sea salt along the gust front. This is, to our knowledge, a first ever report of a maritime corollary
770 to dust producing haboobs (Knippertz et al., 2007; Miller et al., 2008; Seigel and van den
771 Heever, 2012). Particles and meteorological parameters likewise recovered to pre-event levels
772 over the next ten hours.

773
774 While the Sept. 24th event was the largest of its kind, it nevertheless demonstrated patterns
775 similar to over twenty other events: a sharp wind increase and temperature and particle decrease
776 is followed by a lull and eventually precipitation from a cell. When these events occurred in
777 association with isolated cells, we often could observe the entire process from cell formation to
778 cold pool onset and, at times, cell propagation over the site. Investigation of the Sept 24th case,
779 however, led us to a conclusion that despite the short spatial and temporal timescales observed at
780 a receptor site such as the *Vasco*, they are part of a meteorological phenomenon that spans the
781 entire SCS/ES region. Visible and IR satellite imagery of the SCS/ES region for the eighteen

782 hours prior to the September 24th event are presented in Figure 11. At arrival, the cell was only
783 30-50 km along the meridian, with cloud top heights on the order of 12-13 km, well below the 18
784 km tropopause height. Tracing the event back in time with fifteen-minute imagery, we found this
785 system, despite its small size, remained organized for nearly twenty-four hours. Imagery suggests
786 that an isolated thunderstorm that formed near the southern tip of Vietnam/Ho Chi Min City
787 initiated a cold pool southward which eventually embedded within the Southwest monsoonal
788 flow. This cold pool triggered an arc cloud formation that triggered a new set of thunderstorms
789 along the arc, which in turn formed a secondary cold pool and repeated.

790
791 Squall line features such as observed here have been long noted in the literature (e.g., *Trier et al.*,
792 1996), although we have been unable to find cases as long-lived as we found during the cruise.
793 There are some similarities in the radar science literature for mid-latitude systems as “bow
794 echoes” (*Weisman*, 1993). The physics have been studied extensively (e. g., *Weisman and*
795 *Rotunno*, 2004), and the importance of vertical wind shear and the presence of mid-tropospheric
796 dry air behind the storm front is well established. However, the nature of the squall lines in the
797 SCS/ES appears to present an extreme case. Figure 11 (g) and (h) show the MODIS Aqua 670
798 nm visible and cloud top height products for the Sept. 24th event, ten hours before it reached the
799 | *Vasco*. Shown ~~are a pair~~ is a pair of squall lines, with the southern arc being the one that
800 eventually developed most strongly. We find it interesting that, for the most part, the tops of the
801 clouds making up the squall lines reached only 5-6 km, and hence were most likely ice-free.
802 Only isolated cells along the arc became high enough for freezing and further vertical
803 development. However, a review of the satellite loop suggests periodic major storm eruptions
804 along the line, which we surmise help propagate the phenomenon. In comparison, classic mid-
805 latitude bow echoes are very deep along the front; the difference in cloud heights may be related
806 to the relatively larger amounts of CAPE aloft in mid-latitude systems (*Takemi*, 2014), as well as
807 the location of the capping inversion. Long-lived squall lines are known to develop in
808 environments with finely tuned balance between shear and CAPE (*Rotunno et al.*, 1988). The
809 question of whether cold pool propagation is drive by the frequent and relatively shallow
810 | convection or the infrequent troposphere-deep convection is one we plan to study in detail in the
811 near future. From an aerosol point of view, the warm versus cold convective components along
812 the line likely have important ramifications for scavenging or redistribution of aerosol particles

813 in the MBL. Similarly, aerosol impacts on warm versus cold convection are likely different.
814 Aerosol particles have even been hypothesized to influence the cold pools themselves (*Lebo et*
815 *al.*, 2014).

816
817 A second important aspect of these cold pools is their extent across the monsoonal flow. The case
818 experienced by the *Vasco*, while long-lasting, was relatively small in dimension. Frequently,
819 much larger events are observed in our analysis of the satellite data record. An example at the
820 beginning of the research cruise (Sep 18) is presented in Figure 11(i). In this case, younger and
821 | more ~~well~~-developed squall lines are shown, each over 500 km in length. These events were
822 initiated by major thunderstorms over and just offshore of the Malay Peninsula, with
823 overshooting tops of >20 km. They propagated across the entirety of the SCS/ES in under thirty
824 hours. With such wide ranging extent, they must have swept across the entirety of the SCS/ES,
825 perhaps leaving the very clean condition observed in the northern area. Imagery analysis showed
826 the southern portions of these squall lines developing more strongly on their southern half. This
827 suggests that indeed the veering wind shear is supplying energy from the southern domain.

828
829 *4.3 Key Aspects of Chemistry and Particle Microphysics*

830 Detailed analysis of aerosol chemistry, size, and optical properties will be presented in
831 subsequent papers. However, there are key aspects of chemistry and size worth briefly discussing
832 in the context of this regional aerosol source and transport paper. Time series of DRUM sampler
833 derived PM₁ for some key elements are presented in Figure 12: (a) sulfur and potassium and (b)
834 aluminum and vanadium, respectively. Key gas species of CO and benzene are presented in
835 Figure 12(c) as is 2-PenONO₂ (a photo-oxidation product for pentane) and methyl iodide (CH₃I)
836 a marker for biomass burning (*Akagi et al.*, 2011). While aerosol source identification in the
837 | complex Southeast Asian environment can be very involved (see e.g. Atwood [et al.](#), 2013), there
838 are significant features of note. First, though non-sea salt sulfur can be produced by both
839 industrial and biomass burning (particularly peat burning for sulfur), potassium shows significant
840 enrichment during flaming biomass burning (Reid et al., 2005; *Akagi et al.*, 2011). While aerosol
841 source identification in the complex Southeast Asian environment can be very involved (see e.g.
842 | Atwood [et al.](#), 2013), there are significant features of note. First, though non-sea salt sulfur can
843 be produced by both industrial and biomass burning (particularly peat burning for sulfur),

844 potassium shows significant enrichment during flaming biomass burning (*Reid et al.*, 2005;
845 *Akagi et al.*, 2011).

846

847 By and large, sulfur and potassium track with each other over the time period, with a significant
848 enrichment in the post-TC Nesat clear area. Aluminum ~~(not shown)~~, indicative of regional fine
849 dust, or at times fly ash, also tracks sulfur well and potassium quite well, perhaps indicative of
850 soils entrained in biomass burning plumes. As an indicator of industrial or oil combustion,
851 vanadium shows two significant spikes on Sept 26 and Sept 30. This may indicate additional
852 industrial ~~or~~ shipping sources. Based on our trajectory analysis, these cases may very well be
853 influenced from the industrial Singapore-Kuala Lumpur corridor, although high-resolution
854 modeling is required to show this with any certainty. From a gas chemistry point of view, we
855 find that fine aerosol and CO match reasonably well, with the CO enrichment ahead of the Sept
856 24-26 aerosol event perhaps indicative of polluted air masses where particles have been
857 scavenged by precipitation. Benzene, a good and relatively stable indicator of biomass burning
858 and some industrial emissions, also tracks CO, though with perhaps less enrichment in the last
859 day of the cruise. Methyl iodide tracks with potassium as we would expect from a biomass
860 burning trace-r. As 2-PenONO₂ is a photo oxidation product, its presence demonstrates that these
861 plumes are nominally well aged, particularly for the first event. A reduction in 2-PenONO₂ for
862 the last day of the cruise with an enhancement vanadium suggests a change in air mass sources
863 and/or aging. At the same time, the ratio of Ethyne to excess CO can also be used as a
864 photochemical clock for plume aging. While relatively noisy from the cruise, it- ranged from 15
865 for the Sept 18 spike suggesting a fresh source, was consistently lower (2 to 5) for the Sept 28-30
866 event suggested uniformity in fair degree of photochemical aging. Conversely, the Sept 24-26
867 event showed more variability (3 to 8), suggesting more mixed photochemical aging and perhaps
868 sources. Such chemistry must be further analyzed with the aid of numerical models.

869

870 Regarding aerosol size properties, fine-mode size distributions exhibited some variability
871 throughout the cruise (Figure 12; Table 1). Number distributions showed relatively strong trends,
872 with cleaner periods having significantly smaller count modal diameters (~0.11 to 0.24), though
873 curve fits generally converged to count median diameters in the 0.13-0.17 range. Implicit in this
874 is variability in geometric standard deviation, which may have significance in regional aerosol-

875 cloud condensation nuclei studies. Also evident in the number distributions is a frequent shoulder
876 on the large side of the distribution, suggesting differences in aerosol physics and chemistry for
877 the number and volume distributions; not uncommon in mixed environments. Volume median
878 diameters were generally in the 0.27-0.29 μm range for more polluted events, further exhibiting
879 larger overall size. Actual volume modal diameters are slightly larger (~ 0.02) than their curve-fit
880 counterparts. These are typical for both regional pollution and biomass burning environments
881 (*Reid et al.*, 2005; 2013), and are comparable to the AERONET derived VMDs by *Salinas et al.*,
882 (2013) of 0.26-0.40 μm for background and severe smoke haze events and the mean value of
883 0.32 μm by *Reid et al.* (2013) when one considers hygroscopicity.

884

885 An interesting aspect of the particle size and chemistry data for high-frequency events is
886 exemplified by the Sept. 24th cold pool case. Selected thirty-minute average volume distributions
887 taken from the one-minute time series in Figure 10(e) are presented in Figure 13 (c). Thirty-
888 minute average volume distributions leading up to the cold pool event, and twenty-four hours
889 later are nearly identical. In the ten minutes after arrival, we find a $\sim 80\%$ reduction in total
890 particle volume, with another factor of two reduction following the precipitation event. All this
891 time, VMDs remained fairly stable, although a clear increase in larger particle concentrations is
892 observed post wind burst. Between Figure 13 (c) and Figure 10 (d) & (e) we do not see large
893 changes in particle size, but rather only in amplitude. Similarly, ratios of aerosol chemistry are
894 also fairly similar. We can interpret this data and the seven hours before initiation of aerosol
895 population recovery as a sweep of clean air aloft and subsequent further rainout of aerosol
896 particles along the cold front. Given the 3-4 m/s^{-1} marine boundary layer wind speed, over seven
897 hours we expect a roughly 75 km zone of marine boundary layer particles being cleaned out by
898 the event upstream of the *Vasco*. Such a length scale is supported by the satellite images
899 presented in Figure 11, suggesting a ~ 120 -160 km swath was cut by the event.

900

901 5.0 DISCUSSION AND IMPLICATIONS FOR CLOUD and PRECIPITATION STUDIES

902 This paper had three primary objectives: 1) provide a broad overview of the 2011 *Vasco* cruise,
903 including instruments carried, cruise track, and the general characteristics of the regional
904 environment sampled; 2) relate how aerosol properties co-varied with regional meteorological
905 phenomenon and establish the extent to which biomass burning or industrial pollution from the

906 southern Maritime Continent can be transported towards or into the boreal summer southwest
907 | monsoonal trough; and 3) create a narrative based on field data to help bridge climatological
908 indicators commonly used to assess aerosol lifecycle to real world meteorology. To our
909 knowledge, these are the first published aerosol field measurements in the boreal summertime
910 SCS/ES region.

911
912 Central to all meteorological and atmospheric compositional questions for the greater Maritime
913 Continent is the role of convection. As discussed in *Reid et al.* (2012; 2013), if ENSO-induced
914 precipitation anomalies influence the overall interannual variability of burning activity, it is the
915 patterns of convection correlated with MJO indices that best describe the specific timing and
916 lifetime of emissions. Indeed, the importance of the MJO to meteorological phenomenon of the
917 MC cannot be understated (*Zhang*, 2014). Yet we understand very little of the mechanisms of
918 MJO propagation across the region. Embedded in the large scale “forest” point-of-view of
919 ENSO, monsoonal transitions, and the MJO are individual “trees” of specific aerosol and
920 convective events that can be quite diverse in nature, resulting in complex relationships across
921 land, ocean and atmospheric processes.

922
923 From the “forest” point of view, the *Vasco* observed aerosol and meteorology phenomena that
924 largely matched the conceptual model of MC aerosol relationships between fire activity,
925 transport and MJO transport put forth in *Reid et al.* (2012). The entire 2011 burning season was
926 represented by fire activity slightly elevated with what one expects from a moderately-cold
927 ENSO year. Timing of specific burning events was largely consistent with drier phases of the
928 MJO for the western MC (Phases 1 and 5-7). The cruise fortunately took place during an MJO
929 propagation from 3 into 6, and towards the end of a significant burning event, and so sampled
930 some very clean air as well as the highest AOT recorded in the region for that season (Marbel
931 University Mindanao peaked at 500 nm AOT of 0.46, likely as a receptor for southern
932 Kalimantan burning on Sept 28th).

933
934 At the next level of scale, the migration of the MJO into phase 5 around Sept 22 coincided with
935 the development of regional TCs, as described by *Maloney and Hartman* (2001). This included
936 the early-cruise development of a TC in the SCS/ES and the pair of late cruise Category 4 TCs

937 propagating westward across Luzon at the very end of the mission. These TCs clearly enhanced
938 convection along a 2500 km inflow arm spanning the Sumatra/Malay Peninsula to Luzon, and
939 yet also are apparently associated with clear periods and rapid aerosol transport. Indeed, the
940 inflow arm that creates convection, and hence wet deposition, can, at the end of its lifecycle,
941 perhaps rapidly carry more polluted air masses into the SCS/ES and Sulu Seas. In these cases,
942 smoke and anthropogenic emissions from Sumatra and Borneo flowed deep into the greater
943 SCS/ES and Sulu Sea regions. It is quite possible that without TC influence, such events would
944 never have been observed. *Control for TC activity is a likely necessity in any climatological*
945 *analysis of regional aerosol transport.*

946
947 At the finest scales, we were impressed by the nature of coherently-propagating squall line
948 systems across the SCS/ES region, and how these perhaps cut large swaths of aerosol particles
949 out of the environment. Even a cursory view of geostationary data in Fig. 11 shows how
950 convection moves along isolated lines embedded in the SCS/ES monsoonal flow. These features
951 are contrary to the more “bubbling pot” concept of tropical convection in large-scale waves.
952 Examining the entire mission data record, we tracked dozens of lines of convection on the order
953 of 100-500 km in latitudinal length, propagating eastward. Cold pools of storms clearly initiate
954 new convection, which forms another set of cold pools and so on. Veering wind shear allows
955 these storms to cut across aerosol particles transported in the marine boundary layer, effectively
956 removing them from that altitude regime. Perhaps the dry air intrusions in the lower free
957 troposphere from the Indian Ocean provides needed dry air to perpetuate the bow echo-like form
958 observed. But this is speculative at this time and much more research is needed on the physics
959 and conditions that support long squall line phenomenon.

960
961 From an aerosol point of view, the prevalence of high-resolution features like cold pools, and the
962 warm versus cold convective components along the line, likely have important ramifications for
963 scavenging and/or redistribution of aerosol particles in the MBL. Aerosol particles have even
964 been hypothesized to influence the cold pools themselves (*Lebo et al., 2012*), offering up a
965 potential feedback. While there have been many attempts to correlate convective activity with
966 aerosol indicators, such as AOT, organized squall line behavior such as presented here will defeat
967 such a methodology. In the Sept 24th case, the high winds of the cold pool were ahead of the

968 precipitating cell. Thus, particle concentrations were dramatically reduced before the cell arrived.
969 In a study of the influence of cold pool generated dust on the parent convective cell, *Seigel and*
970 *van den Heever* (2012) found the dust had little effect. Vertical transport of the dust was
971 harmlessly ingested at mid-levels. No doubt, the burst of sea salt produced by the cold pools
972 observed on the cruise would meet a similar fate. But, the findings of *Seigel and van den Heever*
973 (2012) have perhaps a more interesting corollary. If wind generated aerosol particles do not have
974 a significant effect, do the aerosol particles ahead of the cold pool also have a lesser effect? Are
975 these particles vertically redistributed and eventually entrained into the clouds at mid-levels as
976 well? Finally, what then is the role of vertical wind shear in bringing aerosol particles from the
977 south into the squall line convection? These questions on aerosol lifecycle and impacts relate
978 back to the convection physics and the nature of clouds within the squall line. From Figure 11(h),
979 cloud tops along the squall line are at 6 km or above, but the efficiency of aerosol scavenging by
980 these features is unknown, although we suspect they are important sinks for regional particles.

981
982 The strong relationships between convection patterns, emissions, and transport have serious
983 implications for regional study of aerosol impacts on clouds and precipitation. Even more so,
984 these process implications propagate further into climate change projections. While the studies of
985 Reid et al., (2012) and Xian et al., (2013) provide a good climatological foundation for aerosol
986 lifecycle, they are nevertheless a substantial smoothing of highly intricate ejection and
987 convection interactions. However, just because relationships are complex does not imply they
988 are fundamentally chaotic. While future papers will describe in more detail the covariance
989 between aerosol particles and convection, it is appropriate to close this paper recalling the
990 covariance between aerosol populations in the MBL and key features in atmospheric soundings
991 in Figure 8. Indeed, the presence of substantial amounts of smoke in the boundary layer is fully
992 intertwined with reduced convection and the presence of dry layers aloft-either through large
993 scale subsidence or dry air. At the same time, these dry layers likely influence the gross type and
994 structure of convection irrespective of aerosol particles as CCN. In future studies, we will
995 attempt to constrain aerosol causality components from thermodynamic forcing of regional
996 convection. At the heart of such an endeavor is understanding what controls convective
997 initiation. Clearly, any aerosol-precipitation study has to account for such complex meteorology.
998 Then, when one considers the implications of aerosol-precipitation feedbacks of a changing

999 | climate, we must consider how such phenomenon as ENSO, monsoonal transitions, the MJO and
1000 | TCs will themselves change. For these phenomenon the community is already challenged to
1001 | perform medium range to seasonal forecasts, let alone develop consistent simulations in climate
1002 | models. Thus, perhaps the most important lesson of this work is that all aerosol-climate
1003 | interaction research for the region is predicated on further advancements of fundamental
1004 | meteorological processes.

1005

1006 6.0 CONCLUSIONS AND HYPOTHESES FOR FUTURE WORK

1007 This paper provides a broad overview of the two-week research cruise of the *Vasco* for
1008 September 17-30, 2011 in the northern Palawan Archipelago of the Philippines. The ship was
1009 stationed on the windward side of the boreal summertime southwest monsoonal trough,
1010 influenced by Marine Boundary Layer (MBL) air originating from the islands surrounding the
1011 Java Sea. Lower free tropospheric air above the MBL largely originated in the Indian Ocean,
1012 passing through and over the Malay Peninsula. Based on the analysis of *Reid et al.* (2012), we
1013 suspected this region's MBL is impacted by anthropogenic pollution and biomass burning
1014 emissions from Indonesia, Malaysia, and Singapore. Given Southeast Asia's ubiquitous cloud
1015 cover, it is difficult to determine by remote sensing what the impact is of anthropogenic activities
1016 on aerosol populations in a region suspected to be vulnerable to aerosol impacts (*Reid et al.*,
1017 2013). What we do know is largely based on modeling studies, which have difficulty with this
1018 most complex of meteorological environments. Hence, this cruise provides the first ever, to our
1019 knowledge, contiguous measurements of the South China Sea/East Sea (SCS/ES) and Sulu Sea
1020 aerosol environment. Based on this cruise, and a subsequent one-month September 2012 *Vasco*
1021 cruise to be reported on later, we observed enough of the environment to study aerosol lifecycle
1022 and pose questions for targeted analysis and testing of cloud impacts. At the very least, the 2011
1023 cruise provides a narrative of real world meteorological phenomena to provide realistic
1024 conceptual models of how the regional aerosol lifecycle relates to the southwest monsoonal
1025 system. In summary, we reported on the following:

1026

1027 1) Boreal summertime 2011 was an El Nino/Southern Oscillation (ENSO) cold "La Nina"
1028 phase year, yet had slightly above-average burning activity for this inter-seasonal state. While

1029 peak burning and aerosol optical thicknesses (AOTs) on Sumatra and Borneo for 2011 occurred
1030 in mid-August, with > 0.8 fine mode 500 nm AOTs recorded by AERONET, the end of the *Vasco*
1031 cruise corresponded to the largest aerosol injection into the Philippines, bringing 500 nm fine
1032 mode AOTs on the order of 0.3 to 0.4.

1033

1034 2) The *Vasco* cruise corresponded with Madden Julian Oscillation (MJO) propagation from
1035 phase 2 to 6, which should enhance burning and transport (*Reid et al.*, 2012). With MJO
1036 propagation came significant tropical cyclone (TC) activity, including the formation of a tropical
1037 storm in the SCS/ES in the early part of the cruise (Haitang), and the propagation of two
1038 Category 4 storms at the very end (Nesat and Nalgae). This TC activity strongly modulated
1039 winds and convection in the greater SCS/ES and Sulu Sea, and thus aerosol regional transport
1040 and lifecycle.

1041

1042 3) Active convective phases associated with TC development and inflow arms demonstrated
1043 extraordinary clean conditions, with Condensation Particle Counter (CPC) concentrations as low
1044 as 150 cm^{-3} , although $300\text{-}500 \text{ cm}^{-3}$ were more typical. Corresponding non-sea salt fine-mode
1045 particle concentrations in these phases were $1 \text{ to } 3 \mu\text{g m}^{-3}$. Coarse sea salt was observed at $4\text{-}8 \mu\text{g}$
1046 m^{-3} . While CALIPSO data during the cruise is unavailable, we suspect that given the regional
1047 veering wind shear, highest particle concentrations were in the MBL. This is supported by
1048 NAAPS model data, as well as climatological analyses and analysis of CALIOP data from
1049 immediately after the cruise period.

1050

1051 4) In between TCs, two significant aerosol injection events were observed, each lasting ~ 2.5
1052 days. The first of these increased CPC particle concentrations to $\sim 1000 \text{ cm}^{-3}$, and average non-
1053 sea salt fine-mode particle concentrations to $\sim 8 \mu\text{g m}^{-3}$. We surmise that long-range transport of
1054 particles reduction of convection to allow long-range transport for this case was induced by a
1055 dry-air intrusion between 800-600 hPa ($\sim 2\text{-}4 \text{ km}$) from the Indian Ocean. This event is perhaps
1056 related to backside MJO subsidence and drying. The aerosol source of this event was likely
1057 southwestern Borneo or with some influence of southern Sumatra. A second more significant
1058 event, with CPC counts as high as 5000 cm^{-3} , occurred in the last days of the cruise when an area
1059 of very clear sky formed between two Category 4 TCs. In this case, significant upper-level

1060 subsidence brought dry air down to below 500 hPa (6 km). High winds in the final stages of the
1061 TC inflow arm leading up to this event may have had a role in its far reaching nature. This
1062 air mass was likely dominated by smoke ejection from southern through southeastern
1063 Kalimantan/Borneo, and perhaps the Sulu Sea. Veering vertical wind shear resulted in aerosol
1064 transport largely in the MBL.

1065

1066 5) While aerosol particle and gas chemistry are subjects of follow-on papers, there are clear
1067 biomass burning signals in both events, particularly in regard to K^+ , CO, benzene and methyl
1068 iodide in the second event. However, in general, air chemistry appears to be a mix of industrial
1069 pollution and biomass burning, with sulfur being the most significant element. Black carbon and
1070 organic carbon ranged from 2% for the cleanest periods, 5-7% for the aerosol events, and up to
1071 12% in Manila bay. Organic carbon was ~30%, increasing to over 50% for the cleanest periods.

1072

1073 6) PCASP derived particle size distributions for more polluted cases was typical for a mix of
1074 pollution and biomass burning, with volume median diameters on the order of 0.27-0.30 μm .
1075 While the PCASP was inoperable for the cleanest periods, more background conditions in the
1076 early part of the cruise showed smaller VMDs, ~0.21 μm .

1077

1078 7) Frequent rapid decreases in particle concentration and temperature, with corresponding
1079 sharp perturbations in winds, were associated with cold pool events. Over twenty such cold pool
1080 events were observed during the cruise. We noted, however, that convection in the SCS/ES
1081 region is often associated with narrow squall lines propagating in the monsoonal flow. In the
1082 most significant case, convection was spawned by a severe thunderstorm over Ho Chi Min City,
1083 whose cold pool propagated southward. Once it reached the southwesterly monsoon, another set
1084 of convection was spawned, creating its own northeastward propagating event. Over the next
1085 twenty-four hours, multiple sets of convection repeated the cycle, leading to arc cloud formations
1086 extending 100-200 km in latitude propagating across the SCS/ES. Upon reaching the *Vasco*, a
1087 one-minute long high wind event (with up to 25 m s^{-1} instantaneous winds) coincided with a
1088 precipitous fall in fine-mode particle concentrations and simultaneous spike in coarse-mode sea
1089 salt. Satellite and measured recovery times suggested a 150 km swath was cut through the marine
1090 boundary layer by this event. While cells up to 20 km high are noted, much of the squall line is

1091 made up of nonfreezing clouds with tops of 6 km. Even a cursory view of regional satellite data
1092 shows these squall lines occur frequently in the southwest monsoonal flow. While only tens of
1093 km wide, they can extend 500 km long across the monsoonal flow, likely supported by low-level
1094 veering winds. These events likely cut swaths of aerosol particles out of the MBL and thus are
1095 likely a major driver of regional aerosol lifecycle. The observation of a cold pool well ahead of
1096 the convection must be considered in aerosol-convection interaction studies.

1097
1098 Based on the above observations, we discussed implications for aerosol, cloud, and precipitation
1099 interaction studies. While aerosol particles are clearly identified by the scientific community as
1100 having a critical role in cloud systems, the covariance between the presence of aerosol particles
1101 and the atmospheric boundary layer state creates an intertwined chicken and egg problem. The
1102 potential for confounding studies is significant. Aerosol injections into the SCS/ES and Sulu Sea
1103 regions were clearly modulated by MJO and TC phenomenon. Dry layers originating in the
1104 Indian Ocean influenced convection thousands of kilometers away. Such features have to be
1105 accounted for in any analysis. However, the significant cloud cover in the region makes data
1106 assimilation for key variables such as water vapor highly problematic. Aerosol observations also
1107 demonstrate substantial clear-sky bias. Higher resolution scales, such as for convection, impart
1108 important fine features and process that are not easily replicated in models. Ultimately, this
1109 investigation highlights how future studies need tight constraints on the overall meteorology,
1110 including high-frequency phenomena such as island ejection of smoke by the sea breeze and cold
1111 pools.

1112
1113 **7.0 ACKNOWLEDGEMENTS**
1114 Organization of this research cruise and associated land base collections required the assistance
1115 of a number of organizations, including the staff of the Office of Naval Research-Global program
1116 office and reservist unit (esp. Joseph Johnson, Blake McBride, Paul Marshall), the Manila
1117 Observatory (esp. Antonia Loyzaga and Fr. Daniel McNamara), US State Department/ Embassy
1118 in Manila (esp. Maria Theresa Villa and Dovas Saulys), and the Naval Postgraduate School (esp.
1119 Richard Lind). We are most grateful to the *Vasco* ship management and crew, managed by
1120 Cosmix Underwater Research Ltd, (esp. Luc Heymans and Annabelle du Parc). We are also
1121 grateful to the host institutions for regional AERONET site deployment and the use of derived
1122 optical thickness data herein. Figure construction was also assisted by Cindy Curtis (NRL) and
1123 Randy Johnson (UND). Funding for this research cruise and analysis was provided from a

1124 number of sources. Vasco time procurement was provided by the NRL 6.1 Base Program via an
1125 ONR Global grant to the Manila Observatory. Funding for NRL scientist deployment and
1126 instrument analysis was provided by the NRL Base Program and ONR 35. Remote sensing and
1127 model analysis was provided by the NASA Interdisciplinary Science Program. Reservist support
1128 was provided by ONR Program 38. The AERONET deployments were supported by the NASA
1129 Radiation Science Program. Gas chemistry was provided by the NASA Tropospheric Chemistry
1130 Program. Author JRC acknowledges the support of NASA Interagency Agreement
1131 NNG13HH10I on behalf of MPLNET and the SEAC⁴RS Science Team.

1132 8.0 REFERENCES:

- 1133 Akagi, S. K., Yokelson, R. J., Weidinger, C., Alvarado, M. J., Reid, J. S., Karl, T., Crouse, J.
1134 D., and Wennberg, P. O., Emission factors for open and domestic biomass burning for use
1135 in atmospheric models, *Atmos. Phys. and Chem.*, 11, 4039–4072, doi:10.5194/acp-11-
1136 4039-2011, 2011
- 1137 Anderson, T. L., Covert, D. S., Marshall, S. F., Laucks, M. L., Charlson, R. J., Waggoner, A. P.,
1138 Ogren, J. A., Caldow, R., Holm, R. L., Quant, F. R., Sem, G. J., Wiedensohler, A.,
1139 Ahlquist, N. A., and Bates, T. S., Performance characteristics of a high-sensitivity three
1140 wavelength, total, backscatter nephelometer, *J. Atm. Ocean. Tech.*, 13, 967-986, 1996.
- 1141 Atkins, N. T., and Wakimoto, R. M., Wet microburst activity over the southeastern United
1142 States: Implications for forecasting, *Weather Forecast.*, 6, 470– 482, 1991.
- 1143 Atwood, S. A., Reid, J. S., Kreidenweis, S. M., Cliff, S. S., Zhao, Y., Lin, N. H., Tsay, S.-C., Chu,
1144 Y.-C., and Westphal, D. L., Size resolved measurements of springtime aerosol particles
1145 over the northern South China Sea, *Atmos. Environ.*, 78, 134-143,
1146 doi:10.1016/j.atmosenv.2012.11.024, 2013a.
- 1147 Atwood, S. A., Reid, J. S., Kreidenweis, S. M., Yu, L. E., Salinas, S. V., Chew, B. N., and
1148 Balasubramanian, R., Analysis of source regions for smoke events in Singapore for the
1149 2009 El Nino burning season, *Atmos. Environ.*, 78, 219-230, doi:
1150 10.1016/j.atmosenv.2013.04.047, 2013b.
- 1151 Bond, T. C., Anderson, T. L., and Campbell, D., Calibration and intercomparison of filter based
1152 measurements of visible light absorption by aerosols, *Aerosol. Sci. Tech.*, 30, 582-600,
1153 doi: 10.1080/027868299304435, 1999.
- 1154 Cahill, T.A., Goodart, C., Nelson, J.W., Eldred, R.A., Nasstrom, J.S., and Feeny, P.J., Design and
1155 evaluation of the DRUM impactor, in: *Proceedings of the International Symposium on*
1156 *Particulate and Multiphase Processes*, Ariman, T. and Veziroglu, T. N. (Eds.), Hemisphere
1157 Publishing Corporation, Washington, D. C., 319-325, 1985
- 1158 Campbell, J. R., Reid, J. S., Westphal, D. L., Zhang, J., Tackett, J. L., Chew, B. N., Welton, E. J.,
1159 Shimizu A., and Sugimoto, N., Characterizing aerosol particle composition and the
1160 vertical profile of extinction and linear depolarization over Southeast Asia and the
1161 Maritime Continent: the 2007-2009 view from CALIOP, *Atmos. Res.*, 122, 520-543,
1162 doi:10.1016/j.atmosres.2012.05.007, 2013.
- 1163 Chang, C.-P., Ding, Y., Lau, N.-C., Johnson, R. H., Wang, B., and Yasunari T., (Eds.), *The Global*
1164 *Monsoon System: Research and Forecast*, 2nd Ed., World Scientific Publishers.,
1165 Singapore, 2011
- 1166 Chang, C.-P., Wang, Z., McBride, J., and Liu, C.-H., Annual cycle of Southeast Asia-Maritime
1167 Continent rainfall and asymmetric monsoon transition. *J. Climate* 18, 287-301, 2005

1168 Chew, B. N., Campbell, J. R., Reid, J. S., Giles, D. M., Welton, E. J., Salinas, S. V., and Liew, S.
1169 C., Tropical cirrus cloud contamination in sun photometer data, *Atmos. Environ.*, 45,
1170 6724-6731, doi: <http://dx.doi.org/10.1016/j.atmosenv.2011.08.017>, 2011

1171 Chew, B. N., Campbell, J. R., Salinas, S. V., Chang, C. W., Reid, J. S., Welton, E. J., Holben, B.
1172 N., and Liew, S. C., Aerosol particle vertical distributions and optical properties over
1173 Singapore, *Atmos. Environ.*, 79, 599-613, doi:
1174 <http://dx.doi.org/10.1016/j.atmosenv.2013.06.026>, 2013

1175 Chow, J. C., Watson, J. G., Pritchett, L. C., Pierson, W. R., Frazier, C. A., and Purcell, R. G., The
1176 DRI thermal/optical analysis system: Description, evaluation and applications in U.S. air
1177 quality studies, *Atmos. Environ.*, 27A, 1185-1201, 1993

1178 [Cinco, T. A., de Guzman, R. G., Hilario, F. D., Wilson, D. M., Long-term trends and extremes](#)
1179 [in observed daily precipitation and near surface air temperature in the Philippines for the](#)
1180 [period 1951-2010, *Atmospheric Research*, 145-146, 12-26,](#)
1181 <http://dx.doi.org/10.1016/j.atmosres.2014.03.025>, 2014.

1182 Clarke, A. D., and Kapustin V., N., The Shoreline Environmental Aerosol Study (SEAS): A
1183 context for marine aerosol measurements influenced by a coastal environment and long-
1184 range transport, *J. Atmos. Ocean. Tech.*, 20, 1351-1361, doi:
1185 [http://dx.doi.org/10.1175/1520-0426\(2003\)020<1351:TSEASS>2.0.CO;2](http://dx.doi.org/10.1175/1520-0426(2003)020<1351:TSEASS>2.0.CO;2), 2003

1186 Colman, J. J., Swanson, A. L., Meinardi, S., Sive, B. B., Blake, D. R., and Rowland, F. S.,
1187 Description of the analysis of a wide range of volatile compounds in whole air samples
1188 collected during PEM-Tropics A and B, *Anal. Chem.*, 73, 3723-3731, 2001

1189 Cruz, F. T., Narisma, G. T., Villafuerte, M. Q., Chua, K. U., and Olaguera, L. M., A
1190 climatological analysis of the southwest monsoon rainfall in the Philippines, *Atmos. Res.*,
1191 112, 609-616, doi:10.1016/j.atmosres.2012.06.010, 2013

1192 Draxler, R. R. HYSPLIT4 users' guide, last accessed March 2012, available at:
1193 <http://purl.access.gpo.gov/GPO/LPS47020>, 2004

1194 Draxler, R. R., and Hess, G. D., Description of the HYSPLIT_4 modeling system. NOAA Tech.
1195 Memo. ERL ARL-224, NOAA Air Resources Laboratory, Silver Spring, MD, 24 pp.,
1196 1997

1197 Draxler, R.R., and Hess, G.D., An overview of the HYSPLIT_4 modeling system of trajectories,
1198 dispersion, and deposition. *Aust. Meteorol. Mag.*, 47, 295-308, 1998

1199 Field, R.D., and Shen, S.S.P., Predictability of carbon emissions from biomass burning in
1200 Indonesia. *J. Geophys. Res.*, 113, G04024, doi:10.1029/2008JG000694, 2008

1201 Field, R.D., van der Werf, G.R., and Shen, S.S.P., Human amplification of drought-induced
1202 biomass burning in Indonesia since 1960, *Nat. Geosci.*, 2, 185-188,
1203 doi:10.1038/NGEO443, 2009

1204 Hamid, E.Y., Kawasakim, Z.-I., and Mardiana, T., Impact of the 1998-1998 El Niño event on
1205 lightning activity over Indonesia. *Geophys. Res. Lett.*, 28, 147-150, 2001

1206 Henintzenberg, J., Covert D. C., and Van Dingenen, R., Size distribution and composition of
1207 marine aerosols: a compilation and review, *Tellus B*, 52, 1104- 1122, 2000

1208 Holben, B. N., Eck, T. F., Slutsker, I., Tanre, D., Buis, J. P., Setzer, A., Vermote, E., Reagan, J. A.,
1209 Kaufman, Y. J., Nakajima, T., Lavenu, F., Jankowiak, I., and Smirnov, A., AERONET - A
1210 federated instrument network and data archive for aerosol characterization, *Remote Sens.*
1211 *Environ.*, 66, 1-16, 1998

1212 Hogan , T.F., and Rosmond, T.E., The description of the U.S. Navy Operational Global
1213 Atmospheric Prediction System's spectral forecast model, *Mon. Wea. Rev.*, 119, 1786-
1214 1815, 1991

1215 Hyer, E. J., and Chew, B. N., Aerosol transport model evaluation of an extreme smoke episode in
 1216 Southeast Asia, *Atmos. Environ.*, 44, 1422-1427, doi:
 1217 <http://dx.doi.org/10.1016/j.atmosenv.2010.01.043>, 2010
 1218 Hyer, E. J., Reid, J. S., Prins, E. M., Hoffman, J. P., Schmidt, C. C., Miettinen, J. I., and Giglio,
 1219 L., Patterns of fire activity over Indonesia and Malaysia from polar and geostationary
 1220 satellite observations, *J. Atmos. Res.*, 122, 504-519, doi:10.1016/j.atmosres.2012.06.011,
 1221 2013
 1222 IPCC, Parry, M. L., Canziani, O. F., Palutikof, J. P., van der Linden, P. J., and Hanson, C. E.
 1223 (Eds.): *Impacts, Adaptation, and Vulnerability, Climate change 2007*, Cambridge
 1224 University Press, United Kingdom, 2007
 1225 Joyce, R. J., Janowiak, J. E., Arkin, P. A., and Xie, P., CMORPH: A method that produces global
 1226 precipitation estimates from passive microwave and infrared data at high spatial and
 1227 temporal resolution, *J. Hydrometeorol.*, 5, 487-503, 2004
 1228 Kahn, R. A., Nelson, D. L., Garay, M., Levy, R. C., Bull, M. A., Martonchik, J. V., Diner, D. J.,
 1229 Paradise, S. R., Wu, D. L., Hansen, E. G., and Remer, L. A., MISR Aerosol product
 1230 attributes, and statistical comparisons with MODIS, *IEEE T. Geosci. Remote*, 47, 4095-
 1231 4114, 2009
 1232 Kalnay, E., Kanamitsu, M., Kistler, R., Collins, W., Deaven, D., Gandin, L., Iredell, M., Saha, S.,
 1233 White, G., Woollen, J., Zhu, Y., Leetmaa, A., and Reynolds, R., The NCEP/NCAR 40-
 1234 year reanalysis project. *Bull. Amer. Meteor. Soc.*, 77, 437-471, doi:
 1235 [http://dx.doi.org/10.1175/1520-0477\(1996\)077<0437:TNYRP>2.0.CO;2](http://dx.doi.org/10.1175/1520-0477(1996)077<0437:TNYRP>2.0.CO;2), 1996
 1236 Knippertz, P., P., Deutscher, C., Kandler, K., Müller, T., Schulz, O., and Schütz L., Dust
 1237 mobilization due to density currents in the Atlas region: Observations from the Saharan
 1238 Mineral Dust Experiment 2006 field campaign, *J. Geophys. Res.*, 112, *D21109*,
 1239 doi:[10.1029/2007JD008774](http://dx.doi.org/10.1029/2007JD008774), 2007
 1240 Langner, A., and Siegert, F., Spatiotemporal fire occurrence in Borneo over a period of 10 years.
 1241 *Global Change Biol.*, 15, 48-62, doi:10.1111/j.1365-2486.2008.01828.x, 2009
 1242 Lebo, Z. J., and Morrison, H., Dynamical effects of aerosol perturbations on simulated idealized
 1243 squall lines, *Mon. Wea. Rev.*, 142, 991-1009, doi: [http://dx.doi.org/10.1175/MWR-D-13-](http://dx.doi.org/10.1175/MWR-D-13-00156.1)
 1244 [00156.1](http://dx.doi.org/10.1175/MWR-D-13-00156.1), 2014
 1245 Lee, S.-S., Feingold, G., and Chuang, P. Y., Effect of aerosol on cloud-environment interactions
 1246 in trade cumulus, *J. Atmos. Sci.*, 69, 3607-3632. doi: [http://dx.doi.org/10.1175/JAS-D-](http://dx.doi.org/10.1175/JAS-D-12-026.1)
 1247 [12-026.1](http://dx.doi.org/10.1175/JAS-D-12-026.1), 2012
 1248 Madden, R. A., and Julian, P. R., Detection of a 40-50 day oscillation in the zonal wind in the
 1249 tropical pacific, *J. Atmos. Sci.*, 28, 702-708, 1971
 1250 Mahmud, M., Mesoscale model simulation of low level equatorial winds over Borneo during the
 1251 haze episode of September 1997, *J. Earth Syst. Sci.*, 118, 295-307, 2009a
 1252 Mahmud, M., Mesoscale equatorial wind prediction in Southeast Asia during a haze episode of
 1253 2005, *Geofizika*, 26, 67-84, 2009b
 1254 Maloney, E. D., and Hartman, D. L., The Madden Julian oscillation, barotropic dynamics, and
 1255 the North Pacific tropical cyclone formation, part 1: Observations, *J. Atmos. Sci.*, 58,
 1256 2545-2558, 2001
 1257 Markowicz, K. M., Flatau, P. J., Kardas, A. E., Remiszewska, J., Stelmaszczyk, K., and Woeste,
 1258 L., Ceilometer retrievals of the boundary layer vertical aerosol extinction structure, *J.*
 1259 *Atmos. Ocean. Tech.*, 25, 928-944, 2008
 1260 Miettinen, J., and Liew, S. C., Degradation and development of peatlands in Peninsular Malaysia

1261 and in the islands of Sumatra and Borneo since 1990, *Land Degrad. Dev.*, 21, 285-296,
1262 doi:10.1002/ldr.976, 2010

1263 Miettinen, J., Shi, C. H., and Liew, S. C., Deforestation rates in insular Southeast Asia between
1264 2000 and 2010, *Global Change Biol.*, 17, 2261-2270, doi:10.1111/j.1365-
1265 2486.2011.02398.x, 2011

1266 Miller, S. D., Hawkins, J. D., Kent, J., Turk, F. J., Lee, T. F., Kuchiauskas, A. P., Richardson, K.,
1267 Wade, R. and Hoffman, C., NexSat: Previewing NPOESS/VIIRS imagery capabilities.
1268 *Bull. Amer. Meteor. Soc.*, 87, 433-446, doi: <http://dx.doi.org/10.1175/BAMS-87-4-433>,
1269 2006

1270 Miller, S. D., Kuciauskas, A. P., Liu, M., Ji, Q., J. S. Reid, J. S., Breed, D. W., Walker, A. L., and
1271 Al Mandoos A., Haboob dust storms of the southern Arabian Peninsula, *J. Geophys. Res.*,
1272 113, D01202, doi:10.1029/2007JD008550, 2008

1273 Moron, V., Robertson, A.W., and Beer, R., Spatial coherence and seasonal predictability of
1274 monsoon onset over Indonesia, *J. Climate*, 22, 840-850, 2009

1275 Nichol, J., Smoke haze in Southeast Asia: A predictable recurrence, *Atmos. Environ.*, 32, 2715-
1276 2716, 1998

1277 O'Neill, N. T., Eck, T. F., Smirnov, A., Holben, B. N., and Thulasiraman, S., Spectral
1278 discrimination of coarse and fine mode optical depth, *J. Geophys. Res.*, 108, 4559,
1279 doi:[10.1029/2002JD002975](http://dx.doi.org/10.1029/2002JD002975), 2003

1280 Parungo, F., Boatman, J. F., Sievering, H., Wilkison, S. W., and Hicks, B. B., Trends in global
1281 marine cloudiness and anthropogenic sulfur. *J. Climate*, 7, 434-440, 1994

1282 Quinn, P. K., Kupustin, V. N., Bates, T. S., and D. S. Covert, Chemical and optical properties of
1283 marine boundary layer aerosol particles of the mid-Pacific in relation to sources and
1284 meteorological transport, *J. Geophys. Res.*, 101, 6931-6951, 1996

1285 Reid, J. S., Brooks, B., Crahan, K. K., Hegg, D. A., Eck, T. F., O'Neill, N., de Leeuw, G., Reid,
1286 E. A., and Anderson K. D., Reconciliation of coarse mode sea-salt aerosol particle size
1287 measurements and parameterizations at a subtropical ocean receptor site, *J. Geophys.*
1288 *Res.*, 111, D02202, doi:10.1029/2005JD006200, 2006

1289 Reid, J. S., Hyer, E. J., Prins, E. M., Westphal, D. L., Zhang, J. L., Wang, J., Christopher, S. A.,
1290 Curtis, C. A., Schmidt, C. C., Eleuterio, D. P., Richardson, K. A., and Hoffman, J. P.,
1291 Global Monitoring and Forecasting of Biomass-Burning Smoke: Description of and
1292 Lessons From the Fire Locating and Modeling of Burning Emissions (FLAMBE)
1293 Program. *IEEE J. Sel. Top. Appl.*, 2, 144-162, doi:10.1109/JSTARS.2009.2027443, 2009

1294 Reid, J. S., Reid, E. A., Walker, A., Piketh, S., Cliff, S., Al Mandoos, A., Tsay, S. C. and Eck, T.
1295 F., Dynamics of southwest Asian dust particle size characteristics with implications for
1296 global dust research, *J. Geophys. Res. Atmos.*, 113, D14212, doi:10.1029/2007JD009752,
1297 2008.

1298 Reid, J. S., Xian, P., Hyer, E. J., Flatau, M. K., Ramirez, E. M., Turk, F. J., Sampson, C. R.,
1299 Zhang, C., Fukada, E. M., and Maloney, E. D., Multi-scale meteorological conceptual
1300 analysis of observed active fire hotspot activity and smoke optical depth in the Maritime
1301 Continent, *Atmos. Chem. Phys.*, 12, 1-31, doi:10.5194/acp-12-1-2012, 2012

1302 Reid, J. S., et al., Observing and understanding the Southeast Asian aerosol system by remote
1303 sensing: An initial review and analysis for the Seven Southeast Asian Studies (7SEAS)
1304 program, *Atmos. Res.*, 122, 403-468, doi:10.1016/j.atmosres.2012.06.005, 2013

1305 Rotunno, R., Klemp, J. B. and Weisman, M. L.: A theory for strong, long-lived squall lines. *J.*
1306 *Atmos. Sci.*, 45, 463-485, 1988.

1307 Rosenfeld, D., TRMM observed first direct evidence of smoke from forest fires inhibiting
1308 rainfall, *Geophys. Res. Lett.*, 26, 3105–3108, doi:10.1029/1999GL006066, 1999
1309 Salinas, S. V., Chew, B. N., Mohamad, M., Mahmud, M., and Liew, S. C., First measurements of
1310 aerosol optical depth and Angstrom exponent number from AERONET's Kuching site,
1311 *Atmos. Environ.*, 78, 231-241, doi:10.1016/j.atmosenv.2013.02.016, 2013
1312 Seigel, R. B., and van den Heever, S. C., Dust lofting and ingestion by supercell storms, *J.*
1313 *Atmos. Sci.*, 69, 1453–1473, doi: <http://dx.doi.org/10.1175/JAS-D-11-0222.1>, 2012
1314 Smirnov, A., Holben, B. N., Giles, D. M., Slutsker, I., O'Neill, N. T., Eck, T. F., Macke, A.,
1315 Croot, P., Courcoux, Y., Sakerin, S. M., Smyth, T. J., Zielinski, T., Zibordi, G., Goes, J. I.,
1316 Harvey, M. J., Quinn, P. K., Nelson, N. B., Radionov, V. F., Duarte, C. M., Losno, R.,
1317 Sciare, J., Voss, K. J., Kinne, S., Nalli, N. R., Joseph, E., Krishna Moorthy, K., Covert, D.
1318 S., Gulev, S. K., Milinevsky, G., Larouche, P., Belanger, S., Horne, E., Chin, M., Remer,
1319 L. A., Kahn, R. A., Reid, J. S., Schulz, M., Heald, C. L., Zhang, J., Lapina, K., Kleidman,
1320 R. G., Griesfeller, J., Gaitley, B. J., Tan, Q., and Diehl, T. L., Maritime aerosol network as
1321 a component of AERONET – first results and comparison with global aerosol models and
1322 satellite retrievals, *Atmos. Meas. Tech.*, 4, 583-597, doi:10.5194/amt-4-583-2011, 2011
1323 Sorooshian, A., Feingold, G., Lebsock, M. D., Jiang, H., and Stephens, G. L., On the
1324 precipitation susceptibility of clouds to aerosol perturbations, *Geophys. Res. Lett.*, 36,
1325 L13803, doi:[10.1029/2009GL038993](http://dx.doi.org/10.1029/2009GL038993), 2009
1326 Takemi, T., Convection and precipitation under various stability and shear conditions: Squall
1327 lines in tropical versus midlatitude environment, *Atmos. Res.*, 142, 111-123.
1328 doi:10.1016/j.atmosres.2013.07.010, 2013
1329 Tian, B., Waliser, D. E., Kahn, R. A., Li, Q., Yung, Y. L., Tyranowski, T., Geogdzhayev, I. V.,
1330 Mishchenko, M. I., Torres, O., Smirnov, A., Does the Madden-Julian Oscillation
1331 influence aerosol variability?, *J. Geophys. Res.*, 113, D12215,
1332 doi:10.1029/2007JD009372, 2008
1333 Tosca, M. G., Randerson, J. T., Zender, C. S., Nelson, D. L., Diner, D. J., and Logan, J. A.,
1334 Dynamics of fire plumes and smoke clouds associated with peat and deforestation fires in
1335 Indonesia. *J. Geophys. Res.*, 116, D08207, doi:10.1029/2010JD015148, 2011
1336 Trier, S. B., Skamarock, W. C., LeMone, M. A., Parsons, D. B., Jorgensen, D. P., Structure and
1337 evolution of the 22 February 1993 TOGA COARE squall line: Numerical simulations, *J.*
1338 *Atmos. Sci.*, 53, 2861–2886, doi: [http://dx.doi.org/10.1175/1520-0469\(1996\)053<2861:SAEOTF>2.0.CO;2](http://dx.doi.org/10.1175/1520-0469(1996)053<2861:SAEOTF>2.0.CO;2), 1996
1339 Tsaknakis, G., Papayannis, A., Kokkalis, P., Amiridis, V., Kambezidis, H. D., Mamouri, R. E.,
1340 Georgoussis, G., and Avdikos, G., Inter-comparison of lidar and ceilometer retrievals for
1341 aerosol and Planetary Boundary Layer profiling over Athens Greece, *Atmos. Meas. Tech.*,
1342 4, 1261-1273, doi:10.5194/amt-4-1261-2011, 2011
1343 van der Kaars, S., Tapper, N., and Cook, E. J., Observed relationships between El-Nino Southern
1344 Oscillation, rainfall variability and vegetation and fire history on Halmahera, Maluku,
1345 Indonesia, *Global Change Biol.*, 16, 1705-1714. doi:10.1111/j.1365-2486.2009.02025.x,
1346 2010
1347 van der Werf, G. R., Randerson, J. T., Collatz, J., Giglio, L., Kasibhatla, P. S., Arellano Jr., A. F.,
1348 Olsen, S. C., and Kasischke, E. S., Continental-scale partitioning of fire emissions during
1349 the 1997 to 2001 El Niño/La Nina period, *Science*, 303, 73-76,
1350 doi:10.1126/science.1090753, 2004
1351

1352 Wakimoto, R. M., Forecasting dry microburst activity over the High Plains, *Mon. Weather Rev.*,
1353 113, 1131–1143, 1985
1354 Wang, J., Gei, C., Yang, Z., Hyer, E., Reid, J. S., Chew, B. N., and Mahmud, M., Mesoscale
1355 modeling of smoke transport over the South Asian maritime continent: vertical
1356 distributions and topographic effect, *Atmos. Res.*, 122, 486-503, 2013
1357 Weisman, M. L., The genesis of severe, long-lived bow echoes, *J. Atmos. Sci.*, 50, 645–670. doi:
1358 [http://dx.doi.org/10.1175/1520-0469\(1993\)050<0645:TGOSLL>2.0.CO;2](http://dx.doi.org/10.1175/1520-0469(1993)050<0645:TGOSLL>2.0.CO;2), 1993
1359 Weisman, M. L., and Rotunno, R., A Theory for Strong Long-Lived Squall Lines Revisited, *J.*
1360 *Atmos. Sci.*, 61, 361–382, doi: [http://dx.doi.org/10.1175/1520-](http://dx.doi.org/10.1175/1520-0469(2004)061<0361:ATFSL>2.0.CO;2)
1361 [0469\(2004\)061<0361:ATFSL>2.0.CO;2](http://dx.doi.org/10.1175/1520-0469(2004)061<0361:ATFSL>2.0.CO;2), 2004
1362 Xian, P., Reid, J. S., Atwood, S. A., Johnson, R., Hyer, E. J., Westphal, D. L., and Sessions, W.,
1363 Smoke transport patters over the Maritime Continent, *Atmos. Res.*, 122, 469-485,
1364 doi:10.1016/j.atmosres.2012.05.006, 2013
1365 Yuan, T., Remer, L. A., Pickering, K. E., Yu H., Observational evidence of aerosol enhancement
1366 of lightning activity and convective invigoration, *Geophys. Res. Lett.*, 38, L04701,
1367 doi:10.1029/2010GL046052, 2011
1368 Yusef, A. A., and Francisco, H., Climate change vulnerability mapping for Southeast Asia,
1369 Economy and Environment Program for Southeast Asia (EEPSEA) report, available at
1370 <http://www.eepsea.net>, last access July 2014, 32 pp, June 2009
1371 Zhang, C., Madden-Julian Oscillation, *Rev. Geophys.*, 43, RG2003,
1372 doi:10.1029/2004RG000158, 2005
1373 Zhang J. L., and Reid, J. S., An analysis of clear sky and contextual biases using an operational
1374 over ocean MODIS aerosol product. *Geophys. Res. Lett.*, 36, L15824,
1375 doi:10.1029/2009GL038723, 2009
1376 Zhang, J. L., Reid, J. S., Westphal, D. L., Baker, N. L., and Hyer, E. J., A system for operational
1377 aerosol optical depth data assimilation over global oceans, *J. Geophys. Res. Atmos.*, 113,
1378 D10208, doi:10.1029/2007JD009065, 2008
1379 Zhang, C., Madden-Julian Oscillation: Bridging Weather and Climate, *Bull. Amer. Meteor. Soc.*,
1380 94, 1849-1870, doi: <http://dx.doi.org/10.1175/BAMS-D-12-00026.1>, 2014
1381 Zuidema, P., Li, Z., Hill, R. J., Bariteau, L., Rilling, B., Fairall, C., Brewer, W. A., Albrecht, B.,
1382 and Hare, J., On trade wind cumulus cold pools. *J. Atmos. Sci.*, 69, 258–280, doi:
1383 <http://dx.doi.org/10.1175/JAS-D-11-0143.1> , 2012
1384

Table 1.

Date	Sample Location	Suspected Source	Mode:CMD: σ_{gn} (μm , μm , N/A)	Mode:VMD: σ_{gv} (μm , μm , N/A)	BC%/OC %	K/S
Sep. 16	Manila Harbor	Metro Manila			12%/19%	0.01
Sep. 17	Manila Bay	Local Bay	0.17:0.16:1.73	0.285:0.30:1.43		0.02
Sep. 17	Outside Manila Bay	Sulu Sea/N. Borneo	0.11/0.17 :0.13:1.37	0:19:0.21:1.52	Bdl/28%	0.08
Sep. 23	Malampaya Sound	Malay Pen. & Sumatra.	N/A	N/A	2%/58%	0.12
Sep. 25	El Nido	SW Borneo	0.17:0.17:1.61	0:285: 0.27:1.36	5%/27%	0.10
Sep. 29	N. El Nido	Southern Borneo	0.24:0.20:1.54	0.31:0.29:1.28	5%/30%	0.29
Sep. 30	Outside Manila Bay	N. Malay Pen. thru Vietnam	0:17:0.18:1.56	0.31:0.28:1.31	7%/31%	0.23

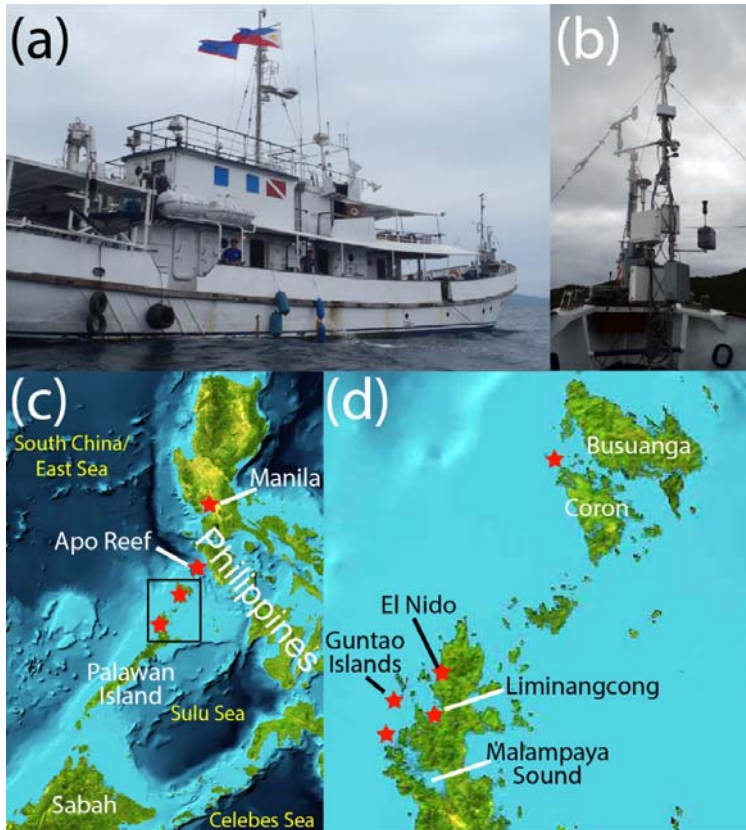


Figure 1. (a) The M/Y Vasco; (b) bow flux tower during the cruise. (c) Map of cruise area, stars mark key areas of sampling. (d) Enlargement of the northern Palawan/Coron Sampling sites.

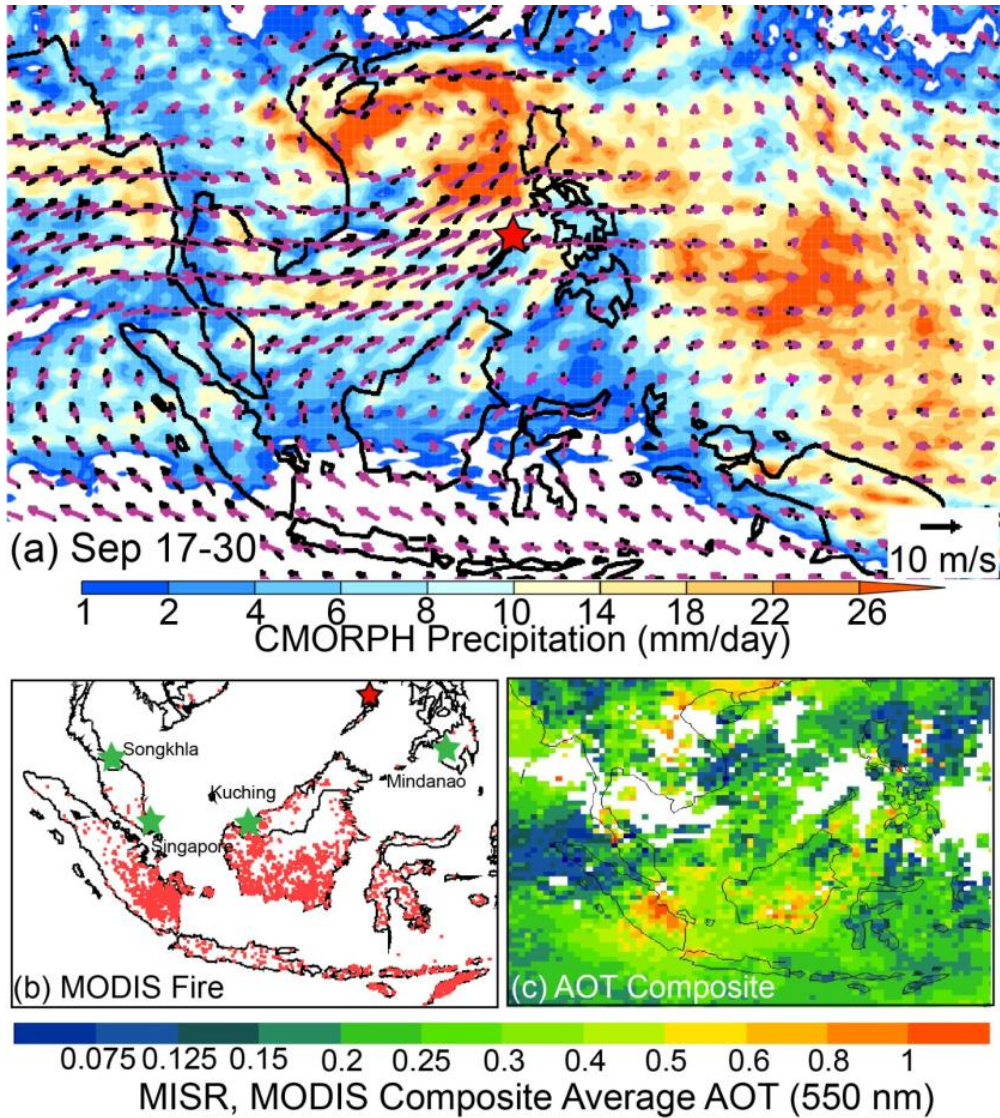


Figure 2. Overview of the aerosol and meteorological environment during the September 17-30 *Vasco* cruise. (a) Surface (black) and 850 hPa (purple) NOGAPS winds overlaid on CMORPH average precipitation rain rates. (b) MODIS Terra+Aqua active fire hotspot detections during the cruise. Overlaid in green stars are key AERONET locations. Red star depicts the El Nido receptor site sampled by the *Vasco*. (c) Composite average MODIS+MISR Aerosol Optical Thickness (AOT).

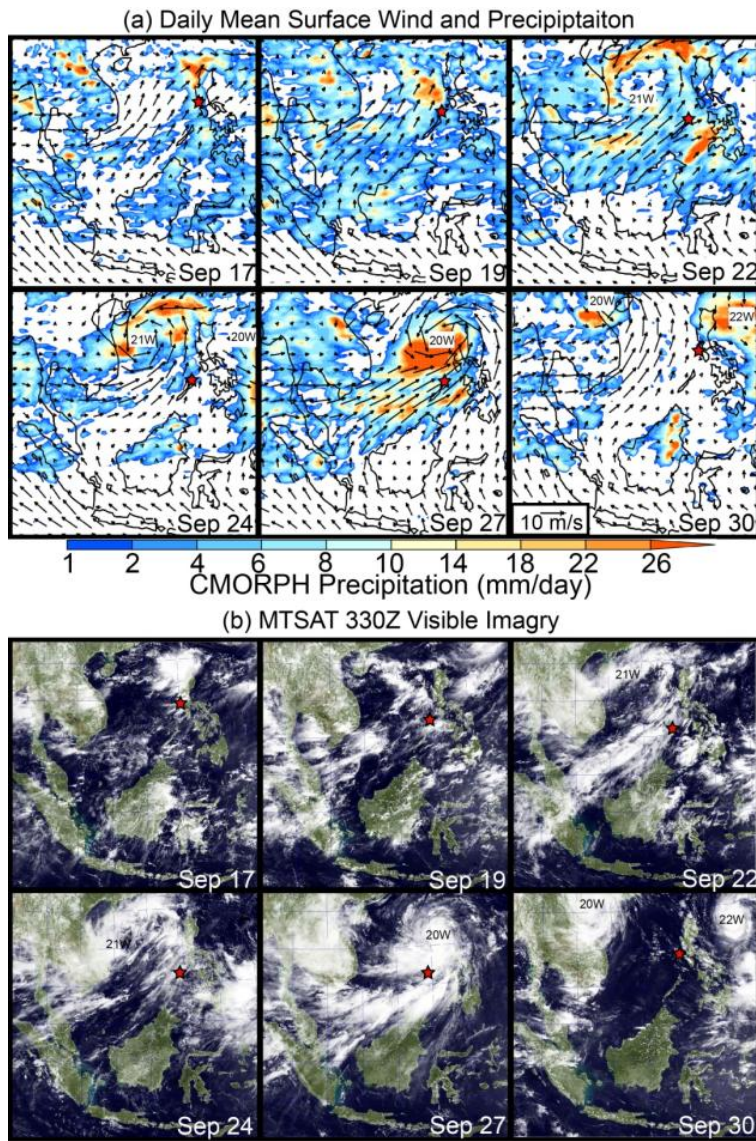


Figure 3. (a) Daily NOGAPS surface winds with CMORPH precipitation for 6 days throughout the cruise demonstrating key meteorological and aerosol modes. (b) Corresponding NexSat 330UTC/1130 LST MTSAT visible imagery with synthetic color background. Ship location at satellite imagery time is located by a red star.

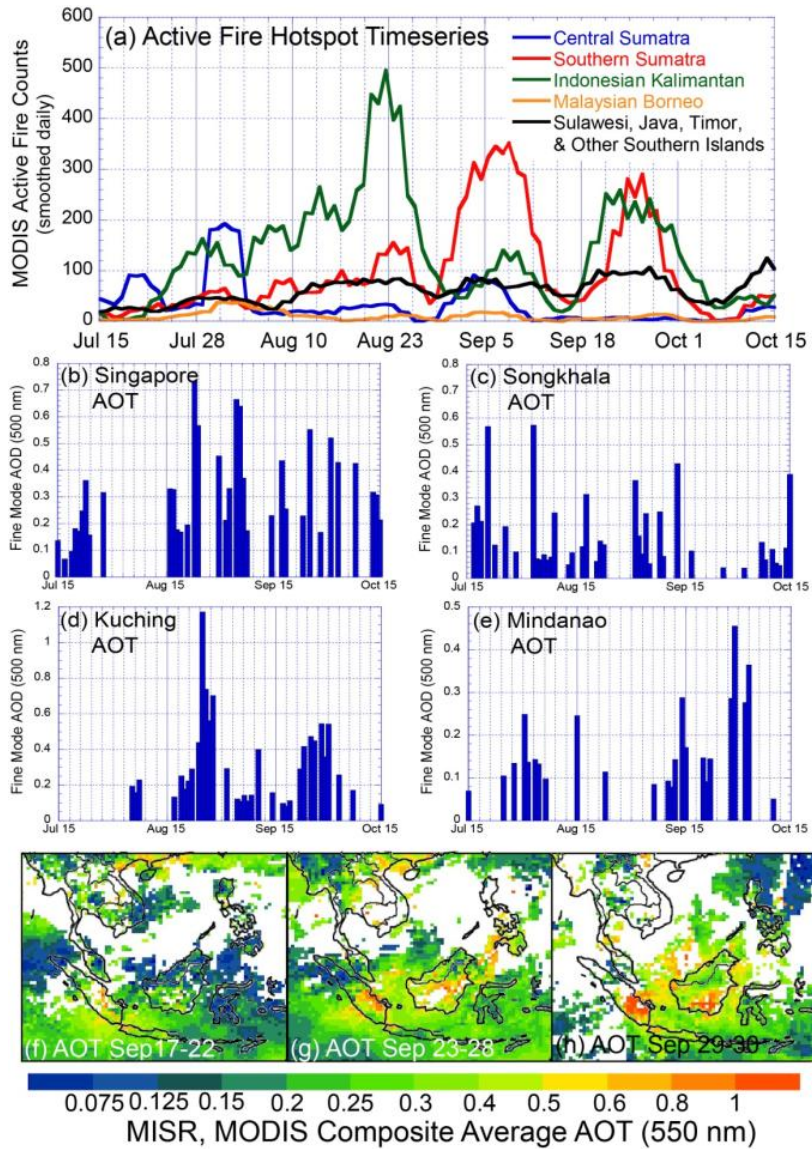


Figure 4. Contextual aerosol data for the 2011 aerosol season. (a) Combined MODIS active fire hotspot prevalence by region. Data is smoothed in a 5 day boxcar filter to help account for orbit. (b)-(e). Level 2 AERONET 500 nm fine mode AOTs for key sites in the Southeast Asian region (marked on Figure 2 (b)) (f)-(h) Combined MODIS 7 MISR satellite AOT analysis for the early, mid and late phases of the cruise.

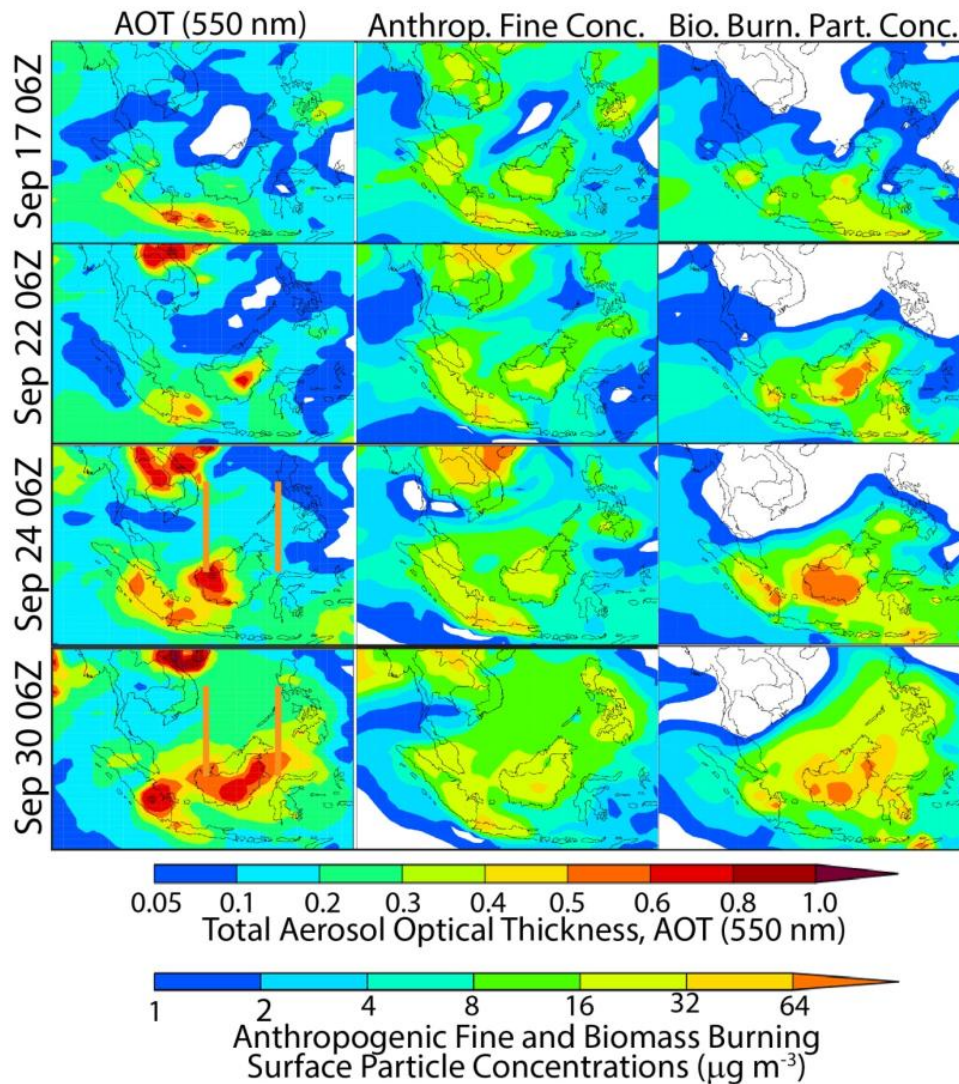


Figure 5. NAAPS 550 nm Aerosol Optical Thickness (AOT) and surface concentrations for fine mode anthropogenic and biomass burning particle concentrations for four key days during the cruise. Satellite data for these four days is also presented in Figure 3. Cross sectional lines for Figure 6 (Sep 24 and 30) are placed on the AOT plot.

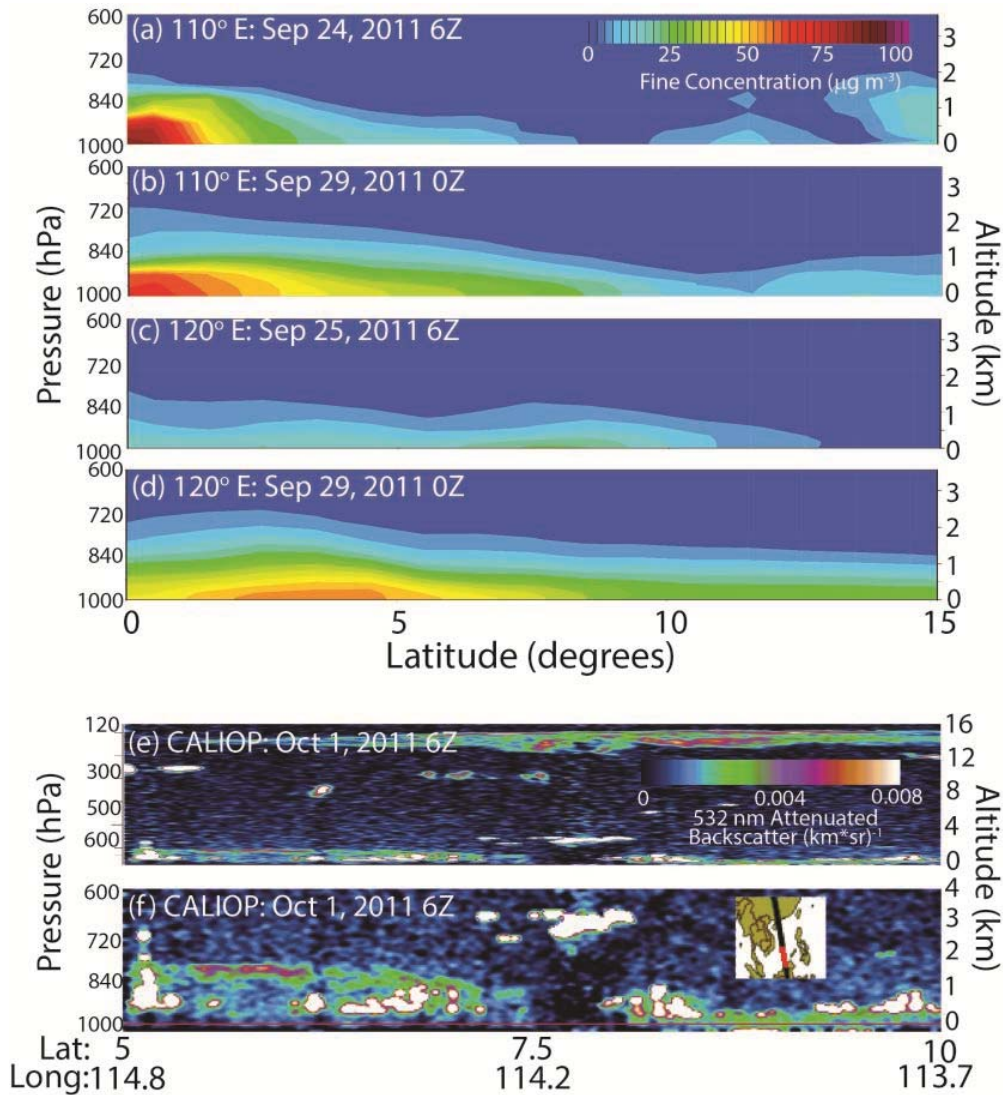


Figure 6. (a)-(d) Meridional cross sections at 110 and 120 east of NAAPS reanalysis total fine mode aerosol particle concentration for the September 25((a) and (c)) and September 29 ((b) and (d)) haze events. (e) CALIOP 532 nm backscatter across the SCS/ES region on Oct 1, 2011. (f) Rescaling of (e) for the lowest 4 km. Included is a map of the CALIPSO track.

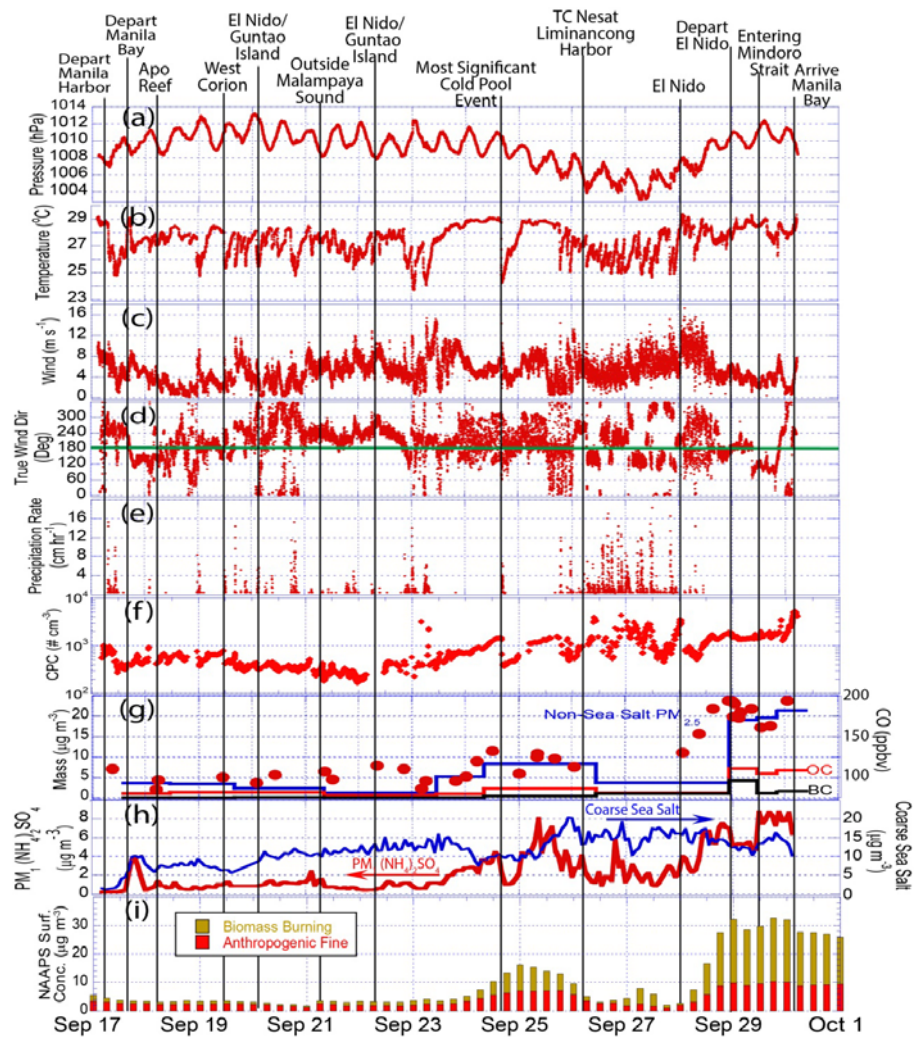


Figure 7. Cruise time series of key meteorological, aerosol and chemistry indicators in 1 minute intervals. Key sampling points and events are marked by vertical lines. (a) Surface pressure (hPa); (b) Ambient air temperature ($^{\circ}\text{C}$); (c) Wind speed (m s^{-1}); (d) True wind direction (degrees); (e) Precipitation rate (cm hr^{-1}); (f) CPC total particle count; (g) Left Axis: PM 2.5 gravimetric mass with sea salt subtracted, and associated organic and black carbon; Right Axis-dots: Can Carbon Monoxide (ppbv); (h) Left Axis-red: DRUM impactor time series of inferred PM1 inferred ammonium sulfate ($\mu\text{g m}^{-3}$); Right Axis-blue: Inferred coarse mode sea salt ($d_p > 0.8 \mu\text{m}$). (i) NAAPS total fine mode particle mass segregated into Anthropogenic (+Biogenic) fine mode and biomass burning.

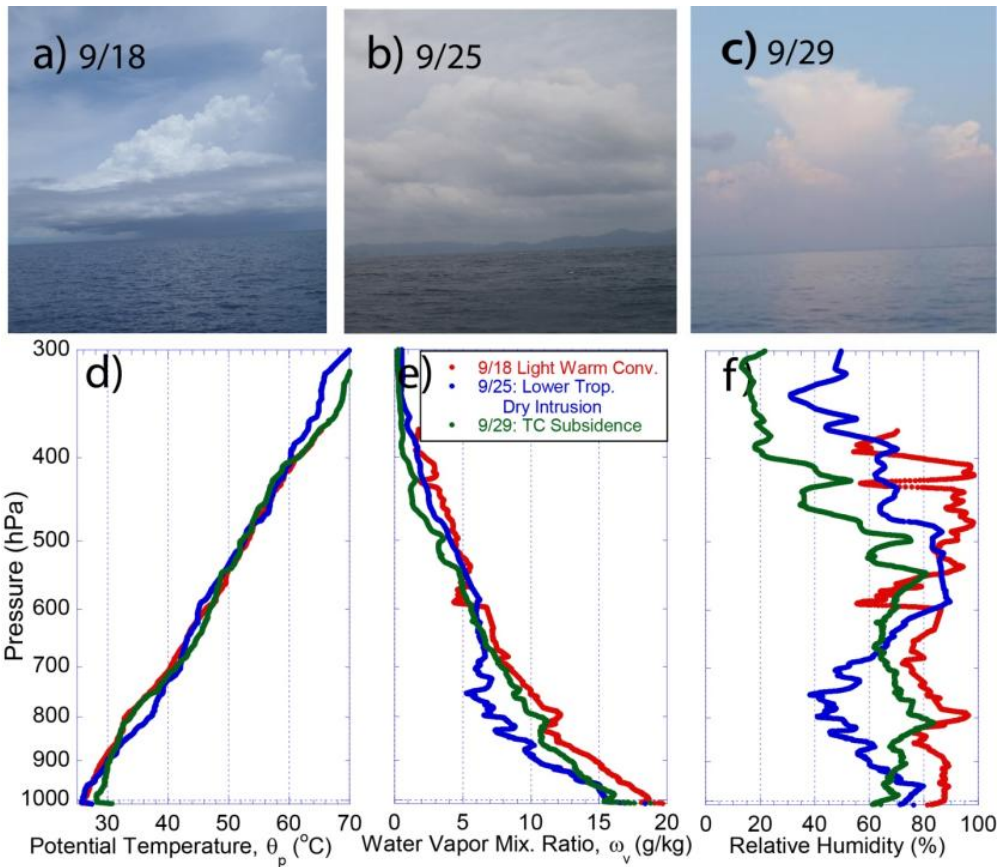


Figure 8. Photographs and corresponding sounding elements for three aerosol regimes during periods of marginal convection. a) Sept. 18th at Apo reef with isolated warm convection in moderately moist conditions; (b) Sept 25th at El Nido with warm non precipitating convection with a lower troposphere dry intrusion during the height of the pollution event; (c) Sept. 29th at the Northern Sulu Sea with isolated deep convection in overall TC induced subsidence during height of biomass burning event. (d), (e) and (f) Corresponding *Vasco* released radiosonde profiles of potential temperature, water vapor mixing ratio, and relative humidity, respectively.

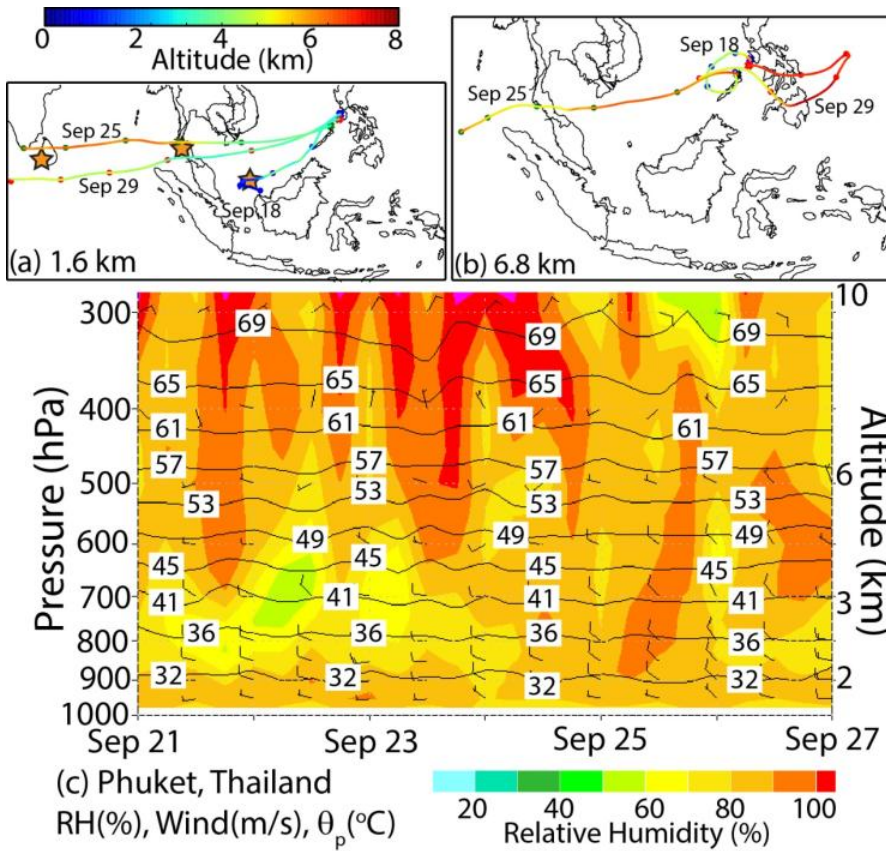


Figure 9. Back trajectories and time height cross sections. (a) & (b) 1.6 km and 6.8 km back trajectories from the *Vasco* for the cases posted in Figure 11. (c) Time height cross section for Phuket, Thailand, of relative humidity-color (RH) with potential temperature isopleths ($^{\circ}\text{C}$). Wind barbs are given with full and half bar at 10 and 5 m/s, respectively.

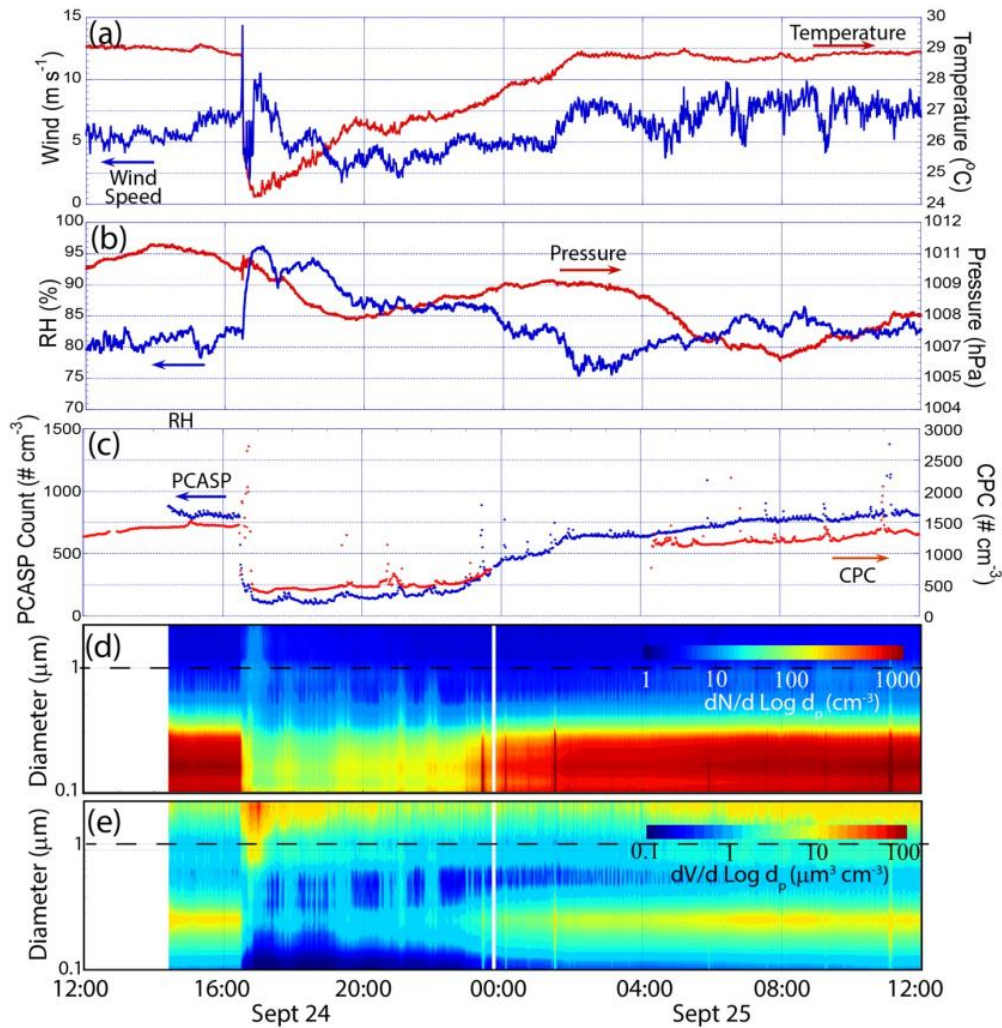


Figure 10. Twenty four hour times series of meteorology and aerosol parameters centered on the September 24th cold pool event. Times are in UTC. (a) 1 minute temperature and wind speed; (b) 1 minute relative humidity and pressure; (c) PCASP and CPC total aerosol particle count; (d) and (e) PCASP number and volume distributions, respectively.

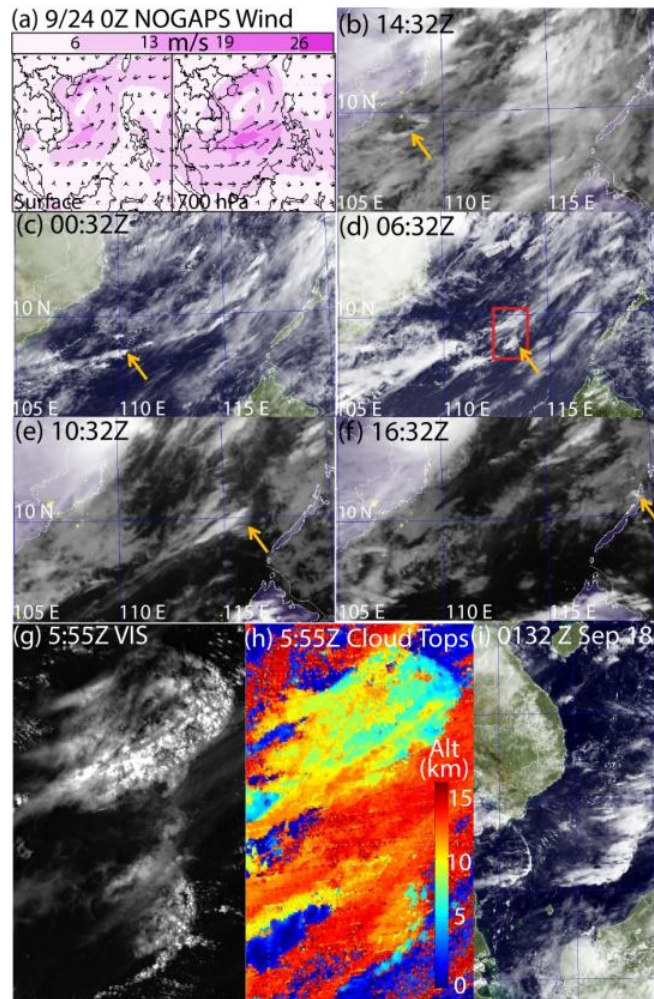


Figure 11. Day visible and night infrared time series of September 24th squall line/cold pool event. (a) Sept 24th 0Z NOGAPS surface and 700 hPa winds at event initiation. (b) Sept. 23rd 14:32Z cold pool arc cloud propagating south from Ho Chi Min City initiated thunderstorm. (c) Sept 24th 00:32Z, convective cell spawned by cold pool, propagating to the NNE; (d) Sept 24th 06:32 Z cold pool from cell in (c); (e) Convective cell spawned by cell in (e); (f) final cell spawned by cold pool from (e) sampled by *Vasco.*; (g) & (h) 250 m MODIS Aqua Ch 1 visible and derived cloud height product respectively. Inset in (d) is the domain. (i) Sep 18 0132 Z MTSAT image of extensive latitudinal dimension of two squall line events.

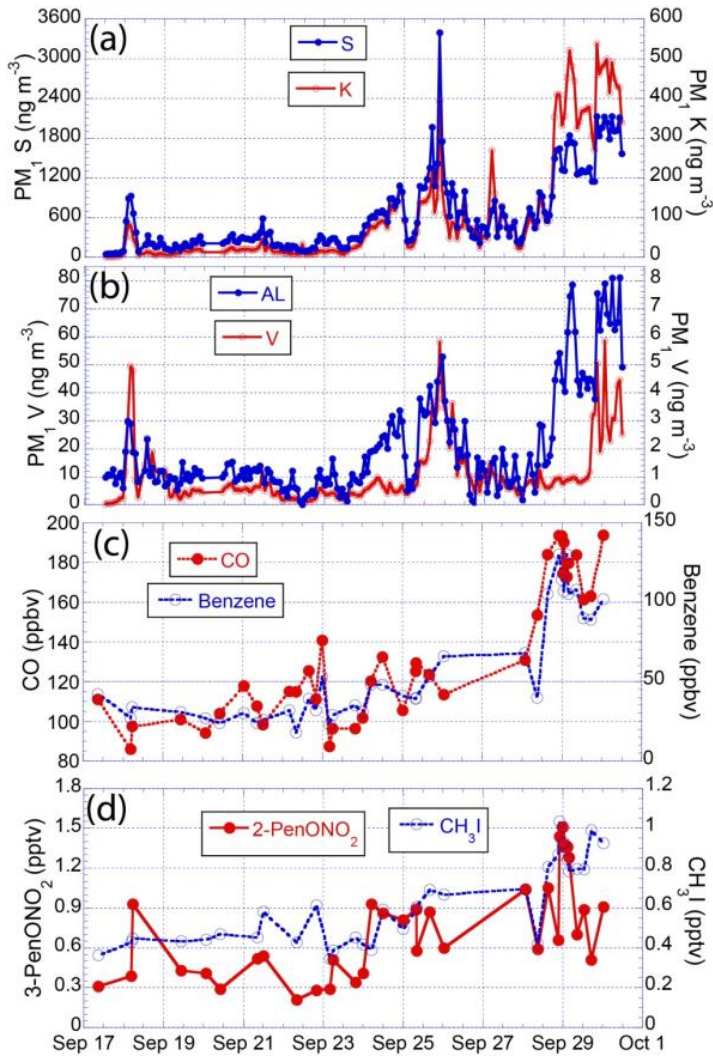


Figure 12. Time series of (key elements and gases. (a) & (b) DRUM time series of Sulfur + Potassium & Aluminum +Vanadium, respectively. (c) Carbon Monoxide and Benzene, both common biomass burning emissions. (d) 2-Pentane Oxy1 Nitrate, a photochemical pentane daughter product and Methyl-Iodide, a halogenated organic specie also emitted by burning, the oceans, and used in agriculture.

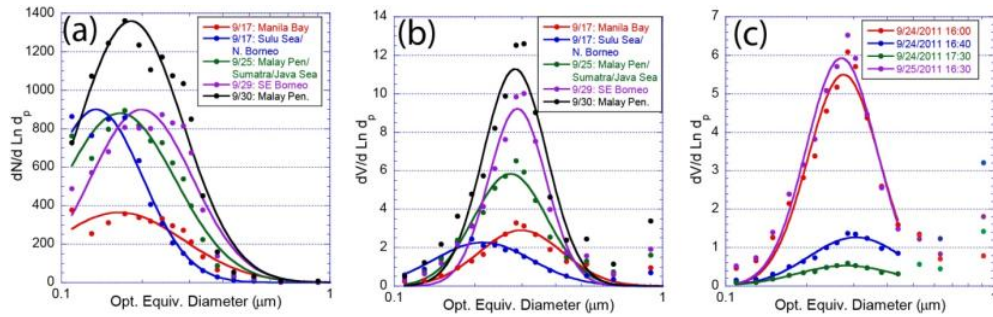


Figure 13. PCASP size distributions for selected regimes. (a) & (b) Number and volume distributions for early, middle and late cruise periods. (c) Volume distributions corresponding to the Sept 24th cold pool event.